AP-1 in the most enriched motifs. There are, however, differences. Mikkelsen discovered PLZF and SRF as novel negative regulators [28] and we found NFIA and NFIB as regulators of adipocyte differentiation—perhaps due to differences in methods. First, we directly compared FAIRE peaks and H3K27ac peaks detected in the Mikkelsen study and found considerable, but not complete, overlap especially in the non-promoter regions: 94% of 10,461 promoter FAIRE peaks and 45% of 27,320 non-promoter FAIRE peaks overlapped H3K27ac in 3T3-L1 on day 0. There may be different classes of enhancer elements that prefer either H3K27ac or open chromatin. Also, we used two parameters to sort motifs: the statistical significance of enrichment (p-value) in either kind of cell type–specific FAIRE peaks; and the motif enrichment ratio between the adipocyte- and preadipocyte-specific FAIRE peaks (see [28]). The combination guarantees significant enrichment of the peaks' motifs and the difference in their number depending on whether they are adipocyte- or preadiocyle-specific. The motifs for PLZF and SRF were not on the top of our list since the p-values were not significant—probably due to relatively lower occurrence, although we also found a significant enrichment ratio of 0.37 and 0.50, respectively. We calculated p-values and the enrichment ratios of the top motifs in the Mikkelsen's study by using our adipocyte- and preadipocyte-specific FAIRE peaks and found general similarity (Figure S10). Overall, both studies notably demonstrate the utility of the combining computational motif analysis and unbiased mapping of regulatory elements in identifying new regulators of adipocyte differentiation.

Siersbæk et al. recently employed DNase-seq to investigate genome-wide change in open chromatin structure at various time points during 3T3-L1 differentiation [6]. They reported dramatic increase in the number of open chromatin sites in the first hours of differentiation. Such regions included what they termed "hot spots" that were bound by multiple adipogenic regulators, facilitating binding of PPARγ and C/EBPα during the late stage of differentiation. We found that the DNaseI hypersensitive sites in 3T3-L1 cells on day 0 or day 6 in the Siersbaek study [6] significantly overlapped the FAIRE peaks on day 0 or day 8 in our study (78.8% and 80.9%, respectively) (Figure S11), suggesting that both methods detect similar open chromatin regions. Although limited amount of motif analyses of the DNase I sites was conducted in their study, we think a combination of motif analysis and DNase-seq should work in a similar way.

The NFI family was identified as site-specific DNA-binding protein that bound to the adenovirus origin of replication [56,57]. Although defects in development of organs such as brain, lung, tooth, bone and skeletal muscle in *Nfia*, *Nfib*, *Nfc* and *Nfix*-deficient mice were documented [64,65,66,67,68,69], no publication has reported direct evidence that NFI family transcription factors are involved in adipogenesis, but it is a reasonable supposition since bone, muscle and adipocytes have a common mesenchymal precursor [70]. Interestingly, Graves et al. demonstrated that NFI was bound to the adipogenic −5.4 kb enhancer region in the aP2 promoter [71], which is the original adipogenic enhancer region where the PPARγ/RXR heterodimer was found to bind and act [72]. The NFI binding motif they examined by gel shift assay [72] was close to the best-characterized PPARγ binding sites in the region, and was also in site 9 (Figure 8A, right panel, site 9), which was indeed bound by NFI in ChIP assay (Figure 8C). Forced overexpression of NFIA in 3T3-L1 cells dramatically induced expression of PPARγ, C/EBPα and aP2 and caused lipid droplet formation before initiation of differentiation. Our ChIP data suggest that activation of these genes by NFIA is through direct binding of NFI to regulatory elements near these genes. In overexpression experiments, NFIB did not activate the adipogenic genes (Figure 7). NFI factors are known to undergo extensive alternative splicing [57]. We speculate that this could be due to truncation of the C-terminus caused by lack of exons 10 and 11 in the NFIB cDNA that we cloned (NM_001113209.1) while the NFIA clone completely matched NM_010905.3. NFI was also implicated in functions of other nuclear receptors such as the androgen receptor (AR), estrogen receptor (ER) and glucocorticoid receptor [4,73,74]. Further studies are necessary to elucidate the mode of action of NFIs and positioning of NFIs in the adipogenic regulatory network.

Materials and Methods

Cell Culture

3T3-L1, NIH-3T3, 3T3-F442A and HEK293T cells were maintained in DMEM, supplemented with 10% FBS. For adipocyte differentiation, two days after confluence, 3T3-L1 cells were treated with dexamethasone (1 μM), IBMX (0.5 mM), and insulin (5 μg/ml) (DMI) for 48 hours, followed by treatment with insulin alone, with medium replacement every two days thereafter. For differentiation of 3T3-F442A, cells were treated with insulin (5 μg/ml) after confluence, with medium replacement every two days.

Animal Studies

All animal works have been conducted according to the institutional guidelines.

Antibodies

Generation of characterization of antibodies for human PPARγ and human RXRα was described previously [24]. Rabbit polyclonal anti-histone H3 trimethyl K4 (ab8580) was from Abcam. Antibodies against CTCF were from Upstate (#07–729). Anti-NFI antibody (H-300) was from Santa Cruz (sc-5567).

FAIRE

FAIRE experiments were performed based on a protocol published by Giresi et al. [7]. Briefly, cells were fixed with 1% formaldehyde for five minutes at room temperature, the fixation stopped by adding 2.5 M glycine (final 125 mM). Fixed cells were scraped and collected in 15 ml tubes (4×10^6 cells/tube) and washed twice with cold PBS, then 8×10^6 cells were re-suspended in 800 μl of MC lysis buffer (10 mM Tris-HCl pH 7.5, 10 mM NaCl, 3 mM $MgCl_2$, 0.5% NP-40) and incubated on ice for ten minutes. After spinning for four minutes at 8000 rpm, the pellet was re-suspended in 400 μl SDS lysis buffer (1% SDS, 10 mM EDTA, 50 mM Tris-HCl pH 8.0, proteinase inhibitor cocktail) and incubated on ice for ten minutes. Glass beads (size, 200 mg) (Polysciences Inc. #05483-250) were added and the DNA was sheared by sonicator. Next, we added 200 μl cold ChIP dilution buffer (0.01% SDS, 1.1% Triton X-100, 1.2 mM EDTA, 16.7 mM Tris-HCl pH 8.0, 167 mM NaCl), and after spinning for one minute at 8,000 rpm, supernatant was transferred to a new 1.5 ml tube. Aliquote was taken, de-crosslinked, purified by phenol/chloroform extraction, and run on a gel to ensure average fragment sizes of 300 bp. Remaining samples were processed three times by phenol/chloroform extraction to recover DNA not bound by nucleosome in the water phase. The samples were de-crosslinked by overnight incubation at 65°C and purified by ethanol precipitation. They were subsequently treated with RNase A (final 50 ug/ml), purified by QIAquick PCR purification kit (Qiagen) and used for subsequent analyses.

Chromatin Immunoprecipitation (ChIP)

ChIP was performed as descried previously [24,75]. For ChIP using anti-PPARγ, RXRα and CTCF antibodies, 3T3-L1 cells

were cross-linked with 1% formaldehyde for ten minutes at room temperature and were prepared for ChIP as described previously. For ChIP using anti-H3K4me3 antibody, the nuclei of 3T3-L1 cells were prepared by centrifugation through a sucrose gradient and were digested with MNase (TaKaRa). After centrifugation, the supernatant was used for ChIP. Sequences of primers used for qPCR were listed in Table S1.

High-Throughput Sequencing and Peak Detection

High-throughput sequencing was performed by using the Genome Analyzer System (GA II) (Illumina) as described elsewhere [76]. In short, we repaired ends of DNA samples, created 3′-dA overhang, ligated Illumina adaptors, size-fractioned the samples by gel extraction and amplified them with 8 cycles of PCR according to the manufacturer's instructions. We then purified the DNA and performed cluster generation and 36 cycles of sequencing on an Illumina cluster station and 1G analyzer following the manufacturer's instructions. Sequences were mapped to the reference murine genome, NCBI build 37 (mm9). Peak detection was performed using Findpeaks 3.1.9.2 [77] with a false discovery rate (FDR) cut-off of 1×10^{-4}. Operations such as intersections, unions, and subtractions of genome regions were performed with a web-based GALAXY genome analysis tool [78,79].

Average Signal Profiling

Average profiling of FAIRE and histone modifications near transcription start sites or FAIRE peaks were generated using "sitepro" in the CEAS package [80].

Adipocyte- and Preadipocyte-Specific FAIRE Peaks

For definition, we first ranked peaks based on signal intensity, which were detected in 3T3-L1 on either day 0 or day 8 with a FDR of 10^{-4}. We then classified each peak into tertiles (high, mid, low) for either day the peak that had the higher percentile (see also the 4-by-4 table in Figure 3B).

Gene Ontology Analysis

Gene ontology annotation analysis was performed using DAVID (ver. 6.7) [38]. The top 2,000 genes were used, sorted by the number and maximum height of the adipocyte-specific FAIRE peaks within a region ±25 kb from TSS. For genes bound by PPARγ, we used the top 931 genes with more than three PPARγ binding sites within a region ±25 kb from TSS. To detect enrichment of specific—rather than general—terms, following the instructions of DAVID's developer, we used GOTERM_BP_4 and GOTERM_BP_5, and sorted result lists by using both fold enrichment and Benjaini p-value [38,81].

Clustering Analysis

Statistical clustering analyses of the PPARγ binding sites and the adipocyte-specific FAIRE peaks were performed as described in references [47,48].

Enriched Motif Analysis

Enrichment analyses of known motifs were performed with AME ver. 4.6.0 in the MEME suite [82]. After removing repeat regions with RepeatMasker [83], DNA sequences from the center 150 bp regions of the top 2,000 cell type–specific FAIRE peaks were analyzed with a fixing partition of 2,000, dinucleotide randomization and p-value threshold of 10^{-4} and p-value report threshold of 0.05. We used the licensed version of TRANSFAC database (Release 2010.4) [51] and the JASPAR CORE database [52].

Motif enrichment ratios (adipocyte-/preadipocytes-specific FAIRE) for motifs in the TRANSFAC or JASPAR CORE database were determined by a method described in reference [28]. Instances of motifs were enumerated in the adipocyte- or preadipocytes-specific FAIRE peaks by using FIMO ver. 4.6.0 in the MEME suite, with a p-value threshold of 10^{-4}, normalized by total nucleotide length. Motif enrichment ratios were determined by dividing the normalized adipocyte enrichment values by preadipocyte values.

MEME ver. 4.3.0 [40] was used to identify de novo motifs over-represented in the adipocyte- or preadipocyte-specific FAIRE peaks and the PPARγ binding sites. After removing repeat regions with RepeatMasker [83], DNA sequences from the center 150 bp regions of the top 800 cell type–specific FAIRE peaks with higher signals were used for the analyses. Identified enriched de novo motifs were next analyzed by TOMTOM in the MEME suite for comparison against a database of known motifs.

Gel Shift Assay and Reporter Assay

The Gel shift assay and luciferase reporter assay were performed as previously described [84,85]. For the luciferase assay, putative PPRE motifs were cloned in tandem (3× or 6×) into pGL3 basic reporter plasmid (Promega) together with the tk minimal promoter. The −5.4 kb aP2 promoter luciferase construct is described in reference [84].

Knockdown of NFIA and NFIB by siRNA in 3T3-L1 Cell Differentiation

The 3T3-L1 cells were transfected with either control siRNA or siRNA for murine NFIA and NFIB (Santa Cruz Biotechnology, sc-37007, sc-36045 and sc-43566, Sigma MISSION siRNA, SASI_Mm02_00309629, 00309630, 00307243, 00307244) by using Lipofectamine RNAiMAX (Invitrogen) just before they reached confluence. Induction of differentiation (the DMI treatment) was started two days after confluence, as described in a method for differentiation of 3T3-L1 cells.

Oil-Red-O Staining

The 3T3-L1 adipocytes were washed with PBS, fixed with formalin for 30 minutes at room temperature, rinsed with 60% isopropanol and stained with oil red O solution—freshly made by mixing 0.5% oil red O in isopropyl alcohol and water (3:2)—and left to sit for one hour; the cells were then washed with water and dried.

mRNA Expression Analysis

Total RNA was isolated using TRIzol reagent (Invitrogen), then 0.5 μg of the total RNA was reverse transcribed using high-capacity cDNA reverse transcription kits (Applied Biosystems #4375222) and random hexamers. Real-time quantitative PCR (SYBR green) analysis was performed on a 7900HT Fast Real-Time PCR System (Applied Biosystems). Primer sequences are listed in Table S1. Expression was normalized to 36B4.

Microarray Analysis

Transcriptome analysis of 3T3-L1 during differentiation by using a GeneChip Mouse Genome 430 2.0 array (Affimetrix) was described previously [24]. Heat maps were generated by using GENOMICA, developed by Yaniv Lubling and Eran Segal at the Weizmann Institute of Science. Microarray data of 3T3-L1 and NIH-3T3 cells used in Figure S11 was obtained from GEO (accession number GSE10246).

Retroviral Expression System

We amplified NFIA and NFIB coding sequences from cDNA prepared from adipocytes using primers listed in Table S1, and cloned them into retroviral pMXs-puro vectors. We also made a dominant negative NFIA that lacks the C-terminal transactivation/repression domain (NFIA-DN) [58]. Plat E cells were transfected with pMXs-puro plasmids using Lipofectamine 2000 (Invitrogen). Culture medium containing viruses after two day incubation was centrifuged at 2,000 rpm for 5 min and supernatant was collected and supplemented with 10 μg/ml polybrene. Conditioned medium with viruses was used to infect 3T3-L1 cells and then selection was started by adding 2 μg/ml puromycin and incubated for 2 days.

Accession Numbers

FAIRE-seq and ChIP-seq raw data are deposited into the DNA data bank of Japan (DDBJ accession number: DRA000378).

Supporting Information

Figure S1 Genomic distribution and characterization of promoter and non-promoter FAIRE peaks in 3T3-L1. (A) Location analysis of FAIRE peaks relative to RefSeq genes in 3T3-L1 (day 0). Promoter FAIRE peaks were defined as those located within +/−500 bp of RefSeq transcription start sites (TSSs). Notably, only 8% of the non-promoter FAIRE peaks were located in the −5 kb proximal promoter region, and the vast majority of them were located in distal regions such as introns and intergenic regions. (B) Average profiles of FAIRE and H3K4me3 signals around the TSSs of genes with high, moderate and low expression levels. Signal intensity from microarray data was used for classification by the signal's expression levels. The X-axis indicates distance from the TSS. (C) Percent fractions of the FAIRE peaks (promoter and non-promoter) that overlapped CTCF binding sites as well as H3K4me1 and H3K4me3 positive regions. (D) Average profiles of FAIRE, H3K4me1, H3K4me3, and H3K27ac signals around the FAIRE peaks in promoter and non-promoter regions. The X-axis shows distance from the center of the FAIRE peaks. The FAIRE peaks located within +/−100 bp from RefSeq TSSs were analyzed for promoter FAIRE peaks. The promoter FAIRE peaks showed H3K4me3(+)/H3K4me1(−) modification whereas the non-promoter FAIRE peaks showed H3K4me3(−)/H3K4me1(+) modification.
(TIF)

Figure S2 Clustering of multiple adipocyte-specific non-promoter FAIRE peaks and PPARγ binding sites near *Mgll*, *Adipor2* and *Slc2a4*. Clusters of multiple adipocyte-specific FAIRE peaks and/or PPARγ binding sites were located in genomic regions near *Mgll* (A), *Adipor2* (B) and *Slc2a4*(Glut4) (C) in 3T3-L1 adipocytes. In some cases—e.g., *Slc2ar4* (Glut4) and *Ybx2* in (C)—multiple genes were located in such regions. Bars below the FAIRE signal represent statistically significant FAIRE positive peaks (FDR$<10^{-4}$). Red asterisks indicate the adipocyte-specific FAIRE peaks on day 8 (see Figure 2B for definition). Blue arrow heads in (B) indicate the PPARγ binding regions in the intron 1 of *Adipor2* tested in Figure 3.
(TIF)

Figure S3 Clustering of multiple adipocyte-specific non-promoter FAIRE peaks and PPARγ binding sites near *Cebpa*, *Srebf1*and *Cidec*. Clusters of multiple adipocyte-specific FAIRE peaks and/or PPARγ binding sites were located in genomic regions near *Cebpa* (A), *Srebf1* (B) and *Cidec* (C).
(TIF)

Figure S4 Binding sites for PPARγ and RXRα in 3T3-L1 cells. (A) De novo motif analysis (MEME) of the center 150 bp of the PPARγ/RXRα binding regions (top 400) in 3T3-L1, day 8. Of note, there is a 5′ extension AGT, which corresponds to the interaction between the PPARγ hinge region and DNA identified by crystal structure analysis [41]. (B) A heat map showing enrichment of PPARγ in the vicinity of genes up-regulated during differentiation. The horizontal bars in the right panel indicate each gene bound by PPARγ (+/−25 kb from TSS, day 8) (C) Ontology analysis with DAVID of genes bound by PPARγ [13].
(TIF)

Figure S5 Co-regulation of neighboring genes during adipocyte differentiation. (A, B) Genomic loci near (A) co-regulated *Mrpl12*, *Slc25a10* and *Gcgr* and (B) co-regulated *Hsd11b1*, *G0s2* and *Lamb3*. Note, there are clusters of the adipocyte-specific FAIRE peaks (asterisks) and the PPARγ binding sites encompassing the co-regulated genes. (C) Microarray analysis showing co-regulation of *Mrpl12*, *Slc25a10* and *Gcgr*, and co-regulation of *Hsd11b1*, *G0s2* and *Lamb3* included in the clusters of multiple adipocyte-specific FAIRE peak and PPARγ binding sites.
(TIF)

Figure S6 Known motif enrichment analysis of the adipocyte- or preadipocyte-specific FAIRE peaks (JASPAR CORE motifs). Enrichment analysis of the adipocyte- (left) and the preadipocyte-specific (right) FAIRE peaks for known motifs in the JASPAR CORE database performed with AME in the MEME suite by the same methods used in Figure 5.
(TIF)

Figure S7 De novo motif analysis of the adipocyte-specific FAIRE peaks. MEME ver. 4.3.0 was used to identify de novo motifs over-represented in the adipocyte- and preadipocyte-specific FAIRE peaks and PPARγ binding sites. After removing repeat regions, DNA sequences from the center 150 bp regions of top 800 cell type–specific FAIRE peaks with higher signals were used for the analyses. Identified enriched de novo motifs were analyzed by TOMTOM in the MEME suite for comparison against a database of known motifs.
(TIF)

Figure S8 Suppression of adipocyte differentiation by knockdown of NFIA and NFIB by using different siRNAs.
(TIF)

Figure S9 Comparison of FAIRE Peaks between undifferentiated 3T3-L1 and NIH-3T3 cells. (A) A heat map showing enrichment of the 3T3-L1- and NIH-3T3-specific FAIRE peaks in the vicinity (+/−25 kb from TSS) of genes sorted by using the ratio of expression levels in 3T3-L1 or NIH-3T3. The FAIRE peaks specific to 3T3-L1 or NIH-3T3 were enriched in the vicinity of genes whose expression levels were higher in 3T3-L1 or NIH-3T3, respectively. (B) Known motif analysis of the 3T3-L1-specific FAIRE peaks (vs NIH-3T3). The binding motif for EBF and PPARγ/RXR were among the top scored motifs.
(TIF)

Figure S10 The enrichment ratios of the top motifs in Mikkelsen's study [28] by using the adipocyte- and preadipocyte-specific FAIRE peaks.
(TIF)

Figure S11 Comparison of DNase-seq in Siersbæk's study [6] and FAIRE-seq peaks near *Klf5*, *Pparg* and *Cebpa* gene. DHS stands for DNase I hypersensitive sites.
(TIF)

Table S1 Sequences of primers.
(DOC)

Acknowledgments

The authors would like to thank: Jason Lieb for providing the FAIRE protocol; the DNA data bank of Japan and Database Center for Life Science (DBCLS) for providing computer resources; all the staff and members of Takashi Kadowaki's lab for technical help and discussion; Kaori Shiina, Shogo Yamamoto, Genta Nagae, Yasuharu Kanki, Atsushi Okabe, Yoichiro Wada, Seitaro Nomura, Kenta Magoori, Takeshi Inagaki, Toshiya Tanaka, and other members of the Laboratory of Systems Biology and Medicine, Research Center, Daizo-Koinuma in the Department of Molecular Pathology; Kenichi Takayama and Satoshi Inoue in the Department of Geriatric Medicine, Yumiko Oishi-Tanaka and Ichiro Manabe in the Department of Cardiovascular Medicine, Kousuke Watanabe and Daiya Takai in the Department of Respiratory Medicine, Graduate School of Medicine, the University of Tokyo—all, for technical help and suggestions.

Author Contributions

Conceived and designed the experiments: H Waki, M Nakamura, T Yamauchi, K Wakabayashi. Performed the experiments: H Waki, M Nakamura, K Wakabayashi, J Yu, L Hirose-Yotsuya, K Take, W Sun, T Aoyama. Analyzed the data: H Waki, M Nakamura, K Wakabayashi, T Fujita, S Tsutsumi, T Yamauchi, M Iwabu, M Okada-Iwabu. Contributed reagents/materials/analysis tools: H Waki, M Nakamura, K Wakabayashi, T Fujita, S Tsutsumi. Wrote the paper: H Waki, M Nakamura. Supervised the design of the experiments: K Ueki, T Kodama, T Yamauchi, S Tsutsumi, J Sakai, H Aburatani, T Kadowaki.

References

1. Lander ES, Linton LM, Birren B, Nusbaum C, Zody MC, et al. (2001) Initial sequencing and analysis of the human genome. Nature 409: 860–921.
2. Wu C (1980) The 5′ ends of Drosophila heat shock genes in chromatin are hypersensitive to DNase I. Nature 286: 854–860.
3. Song L, Crawford GE (2010) DNase-seq: a high-resolution technique for mapping active gene regulatory elements across the genome from mammalian cells. Cold Spring Harb Protoc 2010: pdb prot5384.
4. John S, Sabo PJ, Thurman RE, Sung MH, Biddie SC, et al. (2011) Chromatin accessibility pre-determines glucocorticoid receptor binding patterns. Nat Genet.
5. Heintzman ND, Hon GC, Hawkins RD, Kheradpour P, Stark A, et al. (2009) Histone modifications at human enhancers reflect global cell type–specific gene expression. Nature 459: 108–112.
6. Siersbaek R, Nielsen R, John S, Sung MH, Baek S, et al. (2011) Extensive chromatin remodelling and establishment of transcription factor 'hotspots' during early adipogenesis. Embo J 30: 1459–1472.
7. Giresi PG, Lieb JD (2009) Isolation of active regulatory elements from eukaryotic chromatin using FAIRE (Formaldehyde Assisted Isolation of Regulatory Elements). Methods 48: 233–239.
8. Giresi PG, Kim J, McDaniell RM, Iyer VR, Lieb JD (2007) FAIRE (Formaldehyde-Assisted Isolation of Regulatory Elements) isolates active regulatory elements from human chromatin. Genome Res 17: 877–885.
9. Birney E, Stamatoyannopoulos JA, Dutta A, Guigo R, Gingeras TR, et al. (2007) Identification and analysis of functional elements in 1% of the human genome by the ENCODE pilot project. Nature 447: 799–816.
10. Gaulton KJ, Nammo T, Pasquali L, Simon JM, Giresi PG, et al. (2010) A map of open chromatin in human pancreatic islets. Nat Genet 42: 255–259.
11. Rosen E, Eguchi J, Xu Z (2009) Transcriptional targets in adipocyte biology. Expert Opin Ther Targets 13: 975–986.
12. Waki H, Tontonoz P (2007) Endocrine functions of adipose tissue. Annu Rev Pathol 2: 31–56.
13. Barak Y, Nelson MC, Ong ES, Jones YZ, Ruiz-Lozano P, et al. (1999) PPAR gamma is required for placental, cardiac, and adipose tissue development. Mol Cell 4: 585–595.
14. Kubota N, Terauchi Y, Miki H, Tamemoto H, Yamauchi T, et al. (1999) PPAR gamma mediates high-fat diet-induced adipocyte hypertrophy and insulin resistance. Mol Cell 4: 597–609.
15. Rosen ED, Sarraf P, Troy AE, Bradwin G, Moore K, et al. (1999) PPAR gamma is required for the differentiation of adipose tissue in vivo and in vitro. Mol Cell 4: 611–617.
16. Tontonoz P, Hu E, Spiegelman BM (1994) Stimulation of adipogenesis in fibroblasts by PPAR gamma 2, a lipid-activated transcription factor. Cell 79: 1147–1156.
17. Imai T, Takakuwa R, Marchand S, Dentz E, Bornert JM, et al. (2004) Peroxisome proliferator-activated receptor gamma is required in mature white and brown adipocytes for their survival in the mouse. Proc Natl Acad Sci U S A 101: 4543–4547.
18. Lehmann JM, Moore LB, Smith-Oliver TA, Wilkison WO, Willson TM, et al. (1995) An antidiabetic thiazolidinedione is a high affinity ligand for peroxisome proliferator-activated receptor gamma (PPAR gamma). J Biol Chem 270: 12953–12956.
19. Wu Z, Bucher NL, Farmer SR (1996) Induction of peroxisome proliferator-activated receptor gamma during the conversion of 3T3 fibroblasts into adipocytes is mediated by C/EBPbeta, C/EBPdelta, and glucocorticoids. Mol Cell Biol 16: 4128–4136.
20. Tontonoz P, Spiegelman BM (2008) Fat and beyond: the diverse biology of PPARgamma. Annu Rev Biochem 77: 289–312.
21. Nielsen R, Pedersen TA, Hagenbeek D, Moulos P, Siersbaek R, et al. (2008) Genome-wide profiling of PPARgamma:RXR and RNA polymerase II occupancy reveals temporal activation of distinct metabolic pathways and changes in RXR dimer composition during adipogenesis. Genes Dev 22: 2953–2967.
22. Lefterova MI, Zhang Y, Steger DJ, Schupp M, Schug J, et al. (2008) PPARgamma and C/EBP factors orchestrate adipocyte biology via adjacent binding on a genome-wide scale. Genes Dev 22: 2941–2952.
23. Nakachi Y, Yagi K, Nikaido I, Bono H, Tonouchi M, et al. (2008) Identification of novel PPARgamma target genes by integrated analysis of ChIP-on-chip and microarray expression data during adipocyte differentiation. Biochem Biophys Res Commun 372: 362–366.
24. Wakabayashi K, Okamura M, Tsutsumi S, Nishikawa NS, Tanaka T, et al. (2009) The peroxisome proliferator-activated receptor gamma/retinoid X receptor alpha heterodimer targets the histone modification enzyme PR-Set7/Setd8 gene and regulates adipogenesis through a positive feedback loop. Mol Cell Biol 29: 3544–3555.
25. Hamza MS, Pott S, Vega VB, Thomsen JS, Kandhadayar GS, et al. (2009) De-novo identification of PPARgamma/RXR binding sites and direct targets during adipogenesis. PLoS ONE 4: e4907. doi:10.1371/journal.pone.0004907.
26. Steger DJ, Grant GR, Schupp M, Tomaru T, Lefterova MI, et al. (2010) Propagation of adipogenic signals through an epigenomic transition state. Genes Dev 24: 1035–1044.
27. Lefterova MI, Steger DJ, Zhuo D, Qatanani M, Mullican SE, et al. (2010) Cell-specific determinants of peroxisome proliferator-activated receptor gamma function in adipocytes and macrophages. Mol Cell Biol 30: 2078–2089.
28. Mikkelsen TS, Xu Z, Zhang X, Wang L, Gimble JM, et al. (2010) Comparative epigenomic analysis of murine and human adipogenesis. Cell 143: 156–169.
29. Okamura M, Kudo H, Wakabayashi K, Tanaka T, Nonaka A, et al. (2009) COUP-TFII acts downstream of Wnt/beta-catenin signal to silence PPARgamma gene expression and repress adipogenesis. Proc Natl Acad Sci U S A 106: 5819–5824.
30. Sakabe NJ, Nobrega MA (2010) Genome-wide maps of transcription regulatory elements. Wiley Interdiscip Rev Syst Biol Med. pp 422–437.
31. Phillips JE, Corces VG (2009) CTCF: master weaver of the genome. Cell 137: 1194–1211.
32. Mori T, Sakaue H, Iguchi H, Gomi H, Okada Y, et al. (2005) Role of Kruppel-like factor 15 (KLF15) in transcriptional regulation of adipogenesis. J Biol Chem 280: 12867–12875.
33. Pruitt KD, Tatusova T, Maglott DR (2007) NCBI reference sequences (RefSeq): a curated non-redundant sequence database of genomes, transcripts and proteins. Nucleic Acids Res 35: D61–65.
34. Robertson AG, Bilenky M, Tam A, Zhao Y, Zeng T, et al. (2008) Genome-wide relationship between histone H3 lysine 4 mono- and tri-methylation and transcription factor binding. Genome Res 18: 1906–1917.
35. Heintzman ND, Stuart RK, Hon G, Fu Y, Ching CW, et al. (2007) Distinct and predictive chromatin signatures of transcriptional promoters and enhancers in the human genome. Nat Genet 39: 311–318.
36. Karlsson M, Contreras JA, Hellman U, Tornqvist H, Holm C (1997) cDNA cloning, tissue distribution, and identification of the catalytic triad of monoglyceride lipase. Evolutionary relationship to esterases, lysophospholipases, and haloperoxidases. J Biol Chem 272: 27218–27223.
37. Nishino N, Tamori Y, Tateya S, Kawaguchi T, Shibakusa T, et al. (2008) FSP27 contributes to efficient energy storage in murine white adipocytes by promoting the formation of unilocular lipid droplets. J Clin Invest 118: 2808–2821.
38. Huang da W, Sherman BT, Lempicki RA (2009) Systematic and integrative analysis of large gene lists using DAVID bioinformatics resources. Nat Protoc 4: 44–57.
39. Kliewer SA, Umesono K, Noonan DJ, Heyman RA, Evans RM (1992) Convergence of 9-cis retinoic acid and peroxisome proliferator signalling pathways through heterodimer formation of their receptors. Nature 358: 771–774.
40. Bailey TL, Elkan C (1994) Fitting a mixture model by expectation maximization to discover motifs in biopolymers. Proc Int Conf Intell Syst Mol Biol 2: 28–36.
41. Chandra V, Huang P, Hamuro Y, Raghuram S, Wang Y, et al. (2008) Structure of the intact PPAR-gamma-RXR-alpha nuclear receptor complex on DNA. Nature: 350–356.

42. Schmidt SF, Jorgensen M, Chen Y, Nielsen R, Sandelin A, et al. (2011) Cross-species comparison of C/EBPa and PPARg profiles in mouse and human adipocytes reveals interdependent retention of binding sites. NCBI GEO (Gene Experssion Omnibus): GSE27450.
43. Yamauchi T, Kamon J, Ito Y, Tsuchida A, Yokomizo T, et al. (2003) Cloning of adiponectin receptors that mediate antidiabetic metabolic effects. Nature 423: 762–769.
44. Kadowaki T, Yamauchi T, Kubota N, Hara K, Ueki K, et al. (2006) Adiponectin and adiponectin receptors in insulin resistance, diabetes, and the metabolic syndrome. J Clin Invest 116: 1784–1792.
45. Tsuchida A, Yamauchi T, Takekawa S, Hada Y, Ito Y, et al. (2005) Peroxisome proliferator-activated receptor (PPAR)alpha activation increases adiponectin receptors and reduces obesity-related inflammation in adipose tissue: comparison of activation of PPARalpha, PPARgamma, and their combination. Diabetes 54: 3358–3370.
46. Sun X, Han R, Wang Z, Chen Y (2006) Regulation of adiponectin receptors in hepatocytes by the peroxisome proliferator-activated receptor-gamma agonist rosiglitazone. Diabetologia 49: 1303–1310.
47. Crawford GE, Holt IE, Whittle J, Webb BD, Tai D, et al. (2006) Genome-wide mapping of DNase hypersensitive sites using massively parallel signature sequencing (MPSS). Genome Res 16: 123–131.
48. Stitzel ML, Sethupathy P, Pearson DS, Chines PS, Song L, et al. (2010) Global epigenomic analysis of primary human pancreatic islets provides insights into type 2 diabetes susceptibility loci. Cell Metab 12: 443–455.
49. Ji H, Vokes SA, Wong WH (2006) A comparative analysis of genome-wide chromatin immunoprecipitation data for mammalian transcription factors. Nucleic Acids Res 34: e146.
50. Ebisuya M, Yamamoto T, Nakajima M, Nishida E (2008) Ripples from neighbouring transcription. Nat Cell Biol 10: 1106–1113.
51. Wingender E, Chen X, Hehl R, Karas H, Liebich I, et al. (2000) TRANSFAC: an integrated system for gene expression regulation. Nucleic Acids Res 28: 316–319.
52. Bryne JC, Valen E, Tang MH, Marstrand T, Winther O, et al. (2008) JASPAR, the open access database of transcription factor-binding profiles: new content and tools in the 2008 update. Nucleic Acids Res 36: D102–106.
53. Gupta RK, Arany Z, Seale P, Mepani RJ, Ye L, et al. (2010) Transcriptional control of preadipocyte determination by Zfp423. Nature 464: 619–623.
54. Tominaga S, Yamaguchi T, Takahashi S, Hirose F, Osumi T (2005) Negative regulation of adipogenesis from human mesenchymal stem cells by Jun N-terminal kinase. Biochem Biophys Res Commun 326: 499–504.
55. Hu E, Kim JB, Sarraf P, Spiegelman BM (1996) Inhibition of adipogenesis through MAP kinase-mediated phosphorylation of PPARgamma. Science 274: 2100–2103.
56. Nagata K, Guggenheimer RA, Hurwitz J (1983) Specific binding of a cellular DNA replication protein to the origin of replication of adenovirus DNA. Proc Natl Acad Sci U S A 80: 6177–6181.
57. Gronostajski RM (2000) Roles of the NFI/CTF gene family in transcription and development. Gene 249: 31–45.
58. Namihira M, Kohyama J, Semi K, Sanosaka T, Deneen B, et al. (2009) Committed neuronal precursors confer astrocytic potential on residual neural precursor cells. Dev Cell 16: 245–255.
59. Green H, Kehinde O (1974) Sublines of mouse 3T3 cells that accumulate lipid. Cell 1: 113–116.
60. Jimenez MA, Akerblad P, Sigvardsson M, Rosen ED (2007) Critical role for Ebf1 and Ebf2 in the adipogenic transcriptional cascade. Mol Cell Biol 27: 743–757.
61. Park PJ (2009) ChIP-seq: advantages and challenges of a maturing technology. Nat Rev Genet 10: 669–680.
62. Carroll JS, Liu XS, Brodsky AS, Li W, Meyer CA, et al. (2005) Chromosome-wide mapping of estrogen receptor binding reveals long-range regulation requiring the forkhead protein FoxA1. Cell 122: 33–43.
63. Koinuma D, Tsutsumi S, Kamimura N, Taniguchi H, Miyazawa K, et al. (2009) Chromatin immunoprecipitation on microarray analysis of Smad2/3 binding sites reveals roles of ETS1 and TFAP2A in transforming growth factor beta signaling. Mol Cell Biol 29: 172–186.
64. das Neves L, Duchala CS, Tolentino-Silva F, Haxhiu MA, Colmenares C, et al. (1999) Disruption of the murine nuclear factor I-A gene (Nfia) results in perinatal lethality, hydrocephalus, and agenesis of the corpus callosum. Proc Natl Acad Sci U S A 96: 11946–11951.
65. Steele-Perkins G, Plachez C, Butz KG, Yang G, Bachurski CJ, et al. (2005) The transcription factor gene Nfib is essential for both lung maturation and brain development. Mol Cell Biol 25: 685–698.
66. Steele-Perkins G, Butz KG, Lyons GE, Zeichner-David M, Kim HJ, et al. (2003) Essential role for NFI-C/CTF transcription-replication factor in tooth root development. Mol Cell Biol 23: 1075–1084.
67. Messina G, Biressi S, Monteverde S, Magli A, Cassano M, et al. (2010) Nfix regulates fetal-specific transcription in developing skeletal muscle. Cell 140: 554–566.
68. Plachez C, Lindwall C, Sunn N, Piper M, Moldrich RX, et al. (2008) Nuclear factor I gene expression in the developing forebrain. J Comp Neurol 508: 385–401.
69. Driller K, Pagenstecher A, Uhl M, Omran H, Berlis A, et al. (2007) Nuclear factor I X deficiency causes brain malformation and severe skeletal defects. Mol Cell Biol 27: 3855–3867.
70. Park KW, Halperin DS, Tontonoz P (2008) Before they were fat: adipocyte progenitors. Cell Metab 8: 454–457.
71. Graves RA, Tontonoz P, Ross SR, Spiegelman BM (1991) Identification of a potent adipocyte-specific enhancer: involvement of an NF-1-like factor. Genes Dev 5: 428–437.
72. Tontonoz P, Graves RA, Budavari AI, Erdjument-Bromage H, Lui M, et al. (1994) Adipocyte-specific transcription factor ARF6 is a heterodimeric complex of two nuclear hormone receptors, PPAR gamma and RXR alpha. Nucleic Acids Res 22: 5628–5634.
73. Eeckhoute J, Carroll JS, Geistlinger TR, Torres-Arzayus MI, Brown M (2006) A cell type–specific transcriptional network required for estrogen regulation of cyclin D1 and cell cycle progression in breast cancer. Genes Dev 20: 2513–2526.
74. Jia L, Berman BP, Jariwala U, Yan X, Cogan JP, et al. (2008) Genomic androgen receptor-occupied regions with different functions, defined by histone acetylation, coregulators and transcriptional capacity. PLoS ONE 3: e3645. doi:10.1371/journal.pone.0003645.
75. Kaneshiro K, Tsutsumi S, Tsuji S, Shirahige K, Aburatani H (2007) An integrated map of p53-binding sites and histone modification in the human ENCODE regions. Genomics 89: 178–188.
76. Kawase T, Ohki R, Shibata T, Tsutsumi S, Kamimura N, et al. (2009) PH domain-only protein PHLDA3 is a p53-regulated repressor of Akt. Cell 136: 535–550.
77. Fejes AP, Robertson G, Bilenky M, Varhol R, Bainbridge M, et al. (2008) FindPeaks 3.1: a tool for identifying areas of enrichment from massively parallel short-read sequencing technology. Bioinformatics 24: 1729–1730.
78. Blankenberg D, Von Kuster G, Coraor N, Ananda G, Lazarus R, et al. (2010) Galaxy: a web-based genome analysis tool for experimentalists. Curr Protoc Mol Biol Chapter 19: Unit 19 10 11–21.
79. Goecks J, Nekrutenko A, Taylor J (2010) Galaxy: a comprehensive approach for supporting accessible, reproducible, and transparent computational research in the life sciences. Genome Biol 11: R86.
80. Shin H, Liu T, Manrai AK, Liu XS (2009) CEAS: cis-regulatory element annotation system. Bioinformatics 25: 2605–2606.
81. http://david.abcc.ncifcrf.gov/forum/cgi-bin/ikonboard.cgi?act = ST;f = 3;t = 1311.
82. McLeay RC, Bailey TL (2009) Motif Enrichment Analysis: a unified framework and an evaluation on ChIP data. BMC Bioinformatics 11: 165.
83. Chen N (2004) Using RepeatMasker to identify repetitive elements in genomic sequences. Curr Protoc Bioinformatics Chapter 4: Unit 4 10.
84. Waki H, Park KW, Mitro N, Pei L, Damoiseaux R, et al. (2007) The small molecule harmine is an antidiabetic cell type–specific regulator of PPARgamma expression. Cell Metab 5: 357–370.
85. Davies BS, Waki H, Beigneux AP, Farber E, Weinstein MM, et al. (2008) The expression of GPIHBP1, an endothelial cell binding site for lipoprotein lipase and chylomicrons, is induced by peroxisome proliferator-activated receptor-gamma. Mol Endocrinol 22: 2496–2504.
86. Schmidt SF, Jorgensen M, Chen Y, Nielsen R, Sandelin A, et al. (2011) Cross species comparison of C/EBPalpha and PPARgamma profiles in mouse and human adipocytes reveals interdependent retention of binding sites. BMC Genomics 12: 152.
87. Graves RA, Tontonoz P, Spiegelman BM (1992) Analysis of a tissue-specific enhancer: ARF6 regulates adipogenic gene expression. Mol Cell Biol 12: 1202–1208.

Cell Metabolism
Article

TLE3 Is a Dual-Function Transcriptional Coregulator of Adipogenesis

Claudio J. Villanueva,[1] Hironori Waki,[1] Cristina Godio,[3] Ronni Nielsen,[4] Wen-Ling Chou,[3] Leo Vargas,[5] Kevin Wroblewski,[1] Christian Schmedt,[5] Lily C. Chao,[1] Rima Boyadjian,[1] Susanne Mandrup,[4] Andrea Hevener,[2] Enrique Saez,[3,*] and Peter Tontonoz[1,*]

[1]Howard Hughes Medical Institute and Department of Pathology and Laboratory Medicine
[2]Department of Medicine, Division of Endocrinology
University of California, Los Angeles, Los Angeles, CA 90095, USA
[3]Department of Chemical Physiology, The Skaggs Institute for Chemical Biology, The Scripps Research Institute, La Jolla, CA 92037, USA
[4]Department of Biochemistry and Molecular Biology, University of Southern Denmark, 5230 Odense M, Denmark
[5]Genomics Institute of the Novartis Research Foundation, San Diego, CA 92121, USA
*Correspondence: esaez@scripps.edu (E.S.), ptontonoz@mednet.ucla.edu (P.T.)
DOI 10.1016/j.cmet.2011.02.014

SUMMARY

PPARγ and Wnt signaling are central positive and negative regulators of adipogenesis, respectively. Here we identify the groucho family member TLE3 as a transcriptional integrator of the PPARγ and Wnt pathways. TLE3 is a direct target of PPARγ that participates in a feed-forward loop during adipocyte differentiation. TLE3 enhances PPARγ activity and functions synergistically with PPARγ on its target promoters to stimulate adipogenesis. At the same time, induction of TLE3 during differentiation provides a mechanism for termination of Wnt signaling. TLE3 antagonizes TCF4 activation by β-catenin in preadipocytes, thereby inhibiting Wnt target gene expression and reversing β-catenin-dependent repression of adipocyte gene expression. Transgenic expression of TLE3 in adipose tissue in vivo mimics the effects of PPARγ agonist and ameliorates high-fat-diet-induced insulin resistance. Our data suggest that TLE3 acts as a dual-function switch, driving the formation of both active and repressive transcriptional complexes that facilitate the adipogenic program.

INTRODUCTION

Adipocytes are specialized cells that store excess energy in the form of triglycerides and also serve an endocrine function, secreting adipokines that influence systemic energy homeostasis (Halaas et al., 1995; Steppan et al., 2001; Yamauchi et al., 2001). The formation of adipocytes is dependent on peroxisome proliferator-activated receptor γ (PPARγ) and CCAAT/enhancer binding proteins (C/EBPs), transcription factors that coordinately regulate genes involved in lipid metabolism (Freytag et al., 1994; Tontonoz et al., 1994b). Ectopic expression of PPARγ programs fibroblasts to differentiate into adipocytes (Tontonoz et al., 1994c). Many of the genes characteristic of the differentiated adipocyte are direct targets of PPARγ and/or C/EBPα (Christy et al., 1989; Dalen et al., 2004; Schoonjans et al., 1996; Tontonoz et al., 1994b, 1995). PPARγ is also the therapeutic target of the thiazolidinedione antidiabetic drugs that promote lipid storage and adipokine production in adipose tissue (Lehmann et al., 1995).

Cell-specific gene regulation is driven by DNA-binding factors working in concert with cofactors (Roeder, 2005). Several cofactors have been identified that interact with PPARγ and facilitate its action (Cho et al., 2009; Ge et al., 2002; Gelman et al., 1999; Grøntved et al., 2010; Qi et al., 2003). Interestingly, however, few if any of these factors are regulated components of the differentiation program, i.e., their expression does not change during differentiation. Rather, they act as constitutive factors to permit PPARγ-dependent transcription. In line with this constitutive role, increasing the expression of most PPARγ coactivators above the basal state does not enhance adipogenesis. Expression of PPARγ coactivator-1α (PGC-1α) is highly regulated in brown adipose tissue (BAT) and promotes the expression of genes important for thermogenesis (Puigserver et al., 1998). However, PGC-1α is not believed to play an important role in the development of WAT, and therefore the question of whether coactivators may be regulated components of the white adipose tissue differentiation program remains to be addressed.

The Wnt signaling pathway is a major physiological inhibitor of adipogenesis that is responsible for maintaining preadipocytes in an undifferentiated state (Ross et al., 2000). Wnts are secreted glycoproteins that signal through frizzled receptors leading to the inhibition of the Disheveled/axin/GSK3β complex, thereby preventing the targeted degradation of β-catenin (MacDonald et al., 2009). Accumulation of nuclear β-catenin activates TCF/LEF transcription factors and increases the expression of Wnt target genes (Molenaar et al., 1996). A number of studies have shown that Wnt opposes the actions of PPARγ in adipogenesis (Bennett et al., 2002; Liu and Farmer, 2004). Blocking TCF signaling, for example by ectopic expression of a dominant-negative or conditional deletion of β-catenin in mesenchyme, is sufficient to promote differentiation (Arango et al., 2005; Ross et al., 2000). It has also been suggested that the Wnt signaling pathway is downregulated through the action of PPARγ (Moldes et al., 2003). However, the molecular mechanisms by which Wnt

blocks adipogenesis, as well as those that serve to integrate the PPARγ and Wnt signaling pathways, remain to be elucidated.

Previously, we developed a high-throughput phenotypic screening platform for the identification of modulators of adipogenesis (Waki et al., 2007). We utilized this approach to identify small molecules that drive differentiation through the induction of PPARγ expression (Park et al., 2010; Waki et al., 2007). Here we report the adaptation of this strategy for cDNA library screening and the identification of the groucho family member transducin-like enhancer of split 3 (TLE3) as an adipogenic factor. Despite the fact that TLE proteins have been studied primarily as transcriptional repressors, we find that TLE3 is a potent facilitator of PPARγ activity on its target promoters. We further uncover a mechanism for Wnt-dependent inhibition of adipogenesis and demonstrate that TLE3 antagonizes the Wnt pathway during differentiation. These studies identify TLE3 as a dual-function modulator of adipogenesis that augments PPARγ action and inhibits Wnt signaling.

RESULTS

A High-Throughput Screen for cDNA Modulators of Adipogenesis

We previously validated a phenotype-based high-throughput screen for chemical modulators of adipogenesis (Waki et al., 2007). We modified this approach to screen genome-size cDNA libraries in 384-well format and used it to identify candidate regulators of adipocyte differentiation (Figure S1A). 10T1/2 cells were retrotransfected simultaneously with a luciferase reporter driven by the −5.4 kb aP2 promoter and a collection of 18,292 individually spotted mammalian cDNA expression vectors. The day after transfection, cells were treated with insulin and a PPARγ agonist (rosiglitazone) to induce adipogenic differentiation; luciferase activity was evaluated 4 days later (Figure S1B). The screen was run in duplicate; each plate contained cDNAs encoding PPARγ and C/EBPα as positive controls. Relative intensities were normalized to their respective plate median values, and mean values and standard deviations were calculated for each well from the replicate screens to identify hits. For reconfirmation, a set of 96 cDNAs encoding putative adipogenesis regulators was chosen and reassayed, and luciferase values were normalized to empty vector controls (Figure S1C). A number of cDNAs were identified as activators of aP2-driven luciferase activity in our screen. PPARγ emerged as the most potent activator, and several additional known adipogenic factors were also represented, including C/EBPα, C/EBPδ, early B cell factor 1 (EBF1), and mitogen-activated protein kinase kinase 6 (MAPKK6). Select cDNAs were subsequently evaluated for adipogenic potential by means of stable retroviral transduction of 10T1/2 cells (Figure S1D). TLE3 was chosen for further analysis, as this factor had not previously been linked with adipocyte biology.

TLE3 Expression Is Regulated during Adipocyte Differentiation

We reasoned that if TLE3 was a regulated component of the differentiation program, then its expression should change over the course of differentiation. Indeed, analysis of a time course of 10T1/2 and 3T3-L1 differentiation revealed that TLE3 mRNA expression rose during differentiation and was further enhanced by treatment of the cells with PPARγ agonist (Figures 1A and 1B). A strong increase in TLE3 protein expression was also observed, and again treatment with GW7845 increased its levels (Figure 1C). To determine which component of the differentiation cocktail was primarily responsible for TLE3 induction, 10T1/2 cells were stimulated for 2 days with insulin (I), dexamethasone (D), methylisobutyl xanthine (M), and/or GW7845. TLE3 mRNA and protein expression were found to be responsive to both dexamethasone and PPARγ ligand (Figures 1D and 1E).

We also employed confocal immunofluorescence microscopy to visualize TLE3 expression. In 10T1/2 cells, TLE3 expression colocalized with DAPI staining, consistent with nuclear localization (Figure 1F). Furthermore, the level of TLE3 protein increased robustly in cells induced to differentiate (DMI + GW), and lipid-laden mature adipocytes were consistently TLE3 positive (Figure 1F). In vivo, TLE3 protein expression was readily detected in WAT and BAT, but not in adjacent skeletal muscle (Figure S1E). Interestingly, immunoblot analysis revealed more prominent expression of TLE3 in WAT compared to BAT (Figure S2A). In fractionated mouse WAT, TLE3 was more abundant in adipocytes compared to the stromal-vascular fraction (Figure S2B).

We also investigated whether TLE3 levels were altered in murine models of obesity. We found that ob/ob and db/db mice expressed more TLE3 mRNA in WAT, compared to WT controls (Figures 1G and S2C). Examination of the tissue distribution of the mammalian TLE family of proteins revealed that, although TLE3 was expressed in a number of tissues, its expression was particularly prominent in WAT (Figure 1H).

TLE3 Is a Direct Target of PPARγ

The observation that TLE3 expression increased during differentiation and was responsive to PPARγ agonist administration led us to explore whether TLE3 might be a direct target of PPARγ. We confirmed that short-term treatment of PPARγ-expressing 10T1/2 cells with PPARγ agonist induced TLE3 mRNA (Figure 2A). A similar induction by GW7845 was seen in 3T3-L1 cells. TLE3 expression was also responsive to PPARγ administration in vivo. Treatment of mice with PPARγ (rosiglitazone), but not PPARα (GW7647) or PPARδ (GW742) agonists, induced TLE3 mRNA in WAT and BAT (Figure 2B).

To address whether PPARγ bound directly to the TLE3 promoter, we employed chromatin immunoprecipitation (ChIP) assays combined with deep sequencing (Nielsen et al., 2008). Through analysis of the global PPARγ DNA binding data of Nielsen et al., we identified several putative PPARγ binding regions in the mouse TLE3 locus (Figure 2C). Four of these regions were located more than 50 kb upstream of the transcriptional start site (peaks 1–4), while one was located in an intronic region (peak 5). Sequence analysis revealed that DR-1 sequences were associated with each of these peaks, increasing our confidence that these were likely to be bona fide PPARγ binding sites. To confirm this, we performed ChIP-PCR analysis over the time course of 3T3-L1 adipocyte differentiation. Both RXR and PPARγ bound to the five putative binding sites in the TLE3 genomic region in a differentiation-dependent manner (Figure 2D). No binding was observed with a control region from the myoglobin promoter. These results indicated that TLE3 is a direct PPARγ target gene and suggested that induction of TLE3 by PPARγ

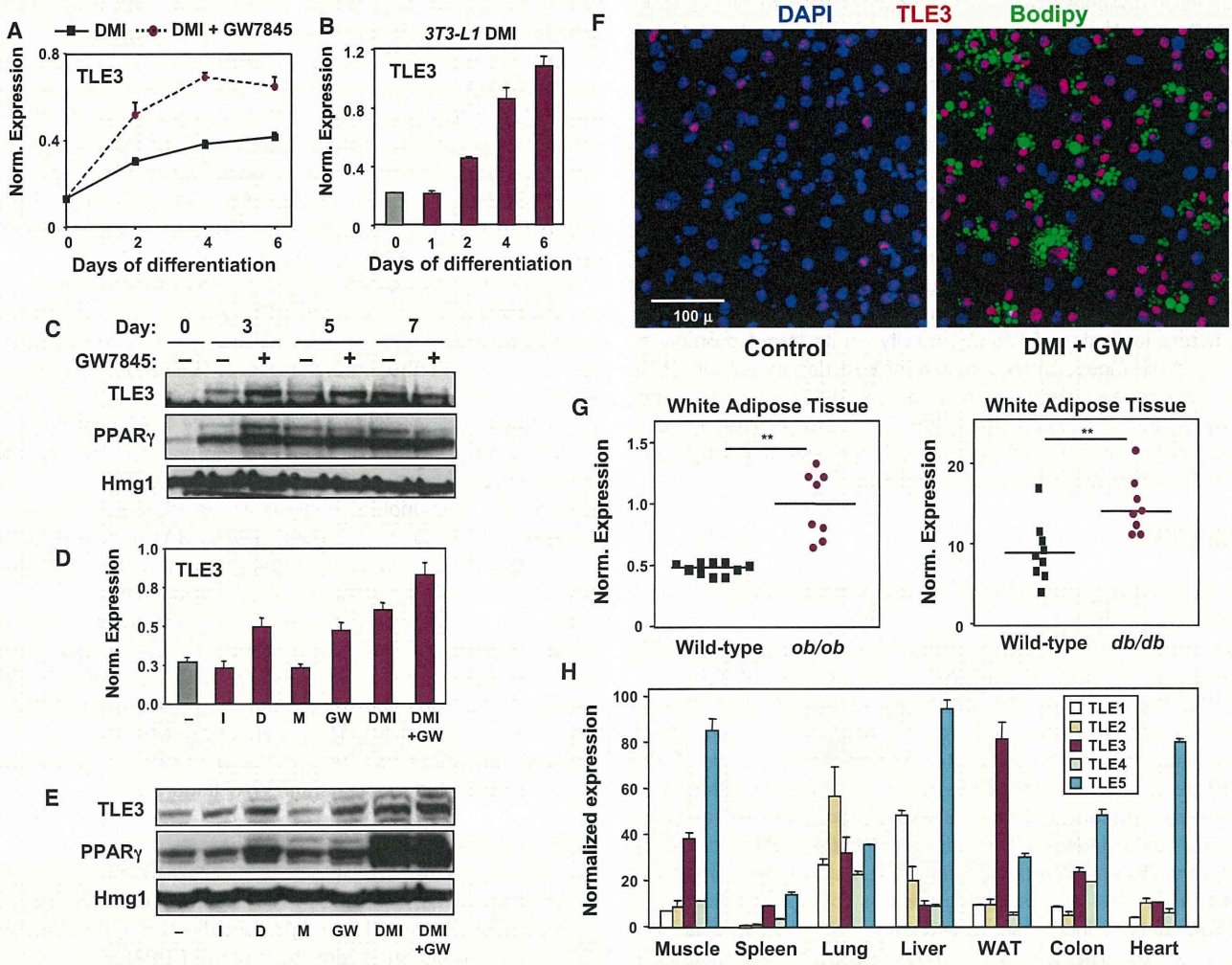

Figure 1. Regulation of TLE3 Expression during Adipocyte Differentiation

(A) Real-time PCR analysis of TLE3 mRNA expression during differentiation of 10T1/2 cells treated with differentiation cocktail (DMI = 1 μM dexamethasone, 0.5 mM IBMX, 5 μg/ml insulin) or DMI and GW7845 (20 nM). mRNA expression in this and all subsequent figures was normalized to 36B4 control.

(B) TLE3 mRNA expression during differentiation of 3T3-L1 preadipocytes. Cells were treated as in (A).

(C) Immunoblot analysis of TLE3 protein expression in 10T1/2 cells treated with DMI plus DMSO (–) or DMI plus GW7845 (20 nM).

(D) Real-time PCR analysis of TLE3 mRNA expression in 10T1/2 cells treated for 2 days with individual components of the differentiation cocktail. D, 1 μM dexamethasone; M, 0.5 mM IBMX; I, 5 μg/ml insulin; GW, 20 nM GW7845.

(E) Immunoblot analysis of total cell lysates from cells treated as in (D).

(F) TLE3 expression visualized by fluorescent confocal microscopy in undifferentiated (control) and differentiated (DMI + 20 nM GW for 4 days) 10T1/2 cells. TLE3 (red) colocalizes with DAPI (blue)-staining nuclei, with highest expression observed in BODIPY (green)-staining adipocytes.

(G) Real-time PCR analysis of TLE3 mRNA expression in epididymal white adipose tissue from ob/ob and db/db mice. N = 8–10 per group, $^{**}p < 0.01$.

(H) Real-time PCR analysis of the relative tissue distribution of mRNAs encoding murine TLE (1–5) family members. Error bars represent mean ± SD. See also Figure S1.

might contribute to a positive feedback loop to promote adipogenesis.

TLE3 Is an Adipogenic Factor that Acts Synergistically with PPARγ

To further validate the adipogenic action of TLE3, we generated stable cell lines. Importantly, these lines expressed TLE3 at only moderately elevated levels, consistent with the degree of TLE3 regulation during adipogenesis. Retroviral TLE3 expression strongly promoted adipocyte differentiation in both 10T1/2 and 3T3-L1 cells, as assessed by oil red O staining (Figure 3A). We also assayed the activity of TLE5, which lacks a WD40 domain and is postulated to act as a dominant negative (Chen and Courey, 2000). TLE5 expression did not affect differentiation, suggesting that a functional WD40 domain is required for the adipogenic effect. Prior studies have identified loss-of-function groucho point mutations (Jennings et al., 2006). Introduction of a loss-of-function point mutation in the WD40 domain (V708D) blocked the ability of TLE3 to stimulate adipogenesis (Figure S3B). Gene expression analysis confirmed increased

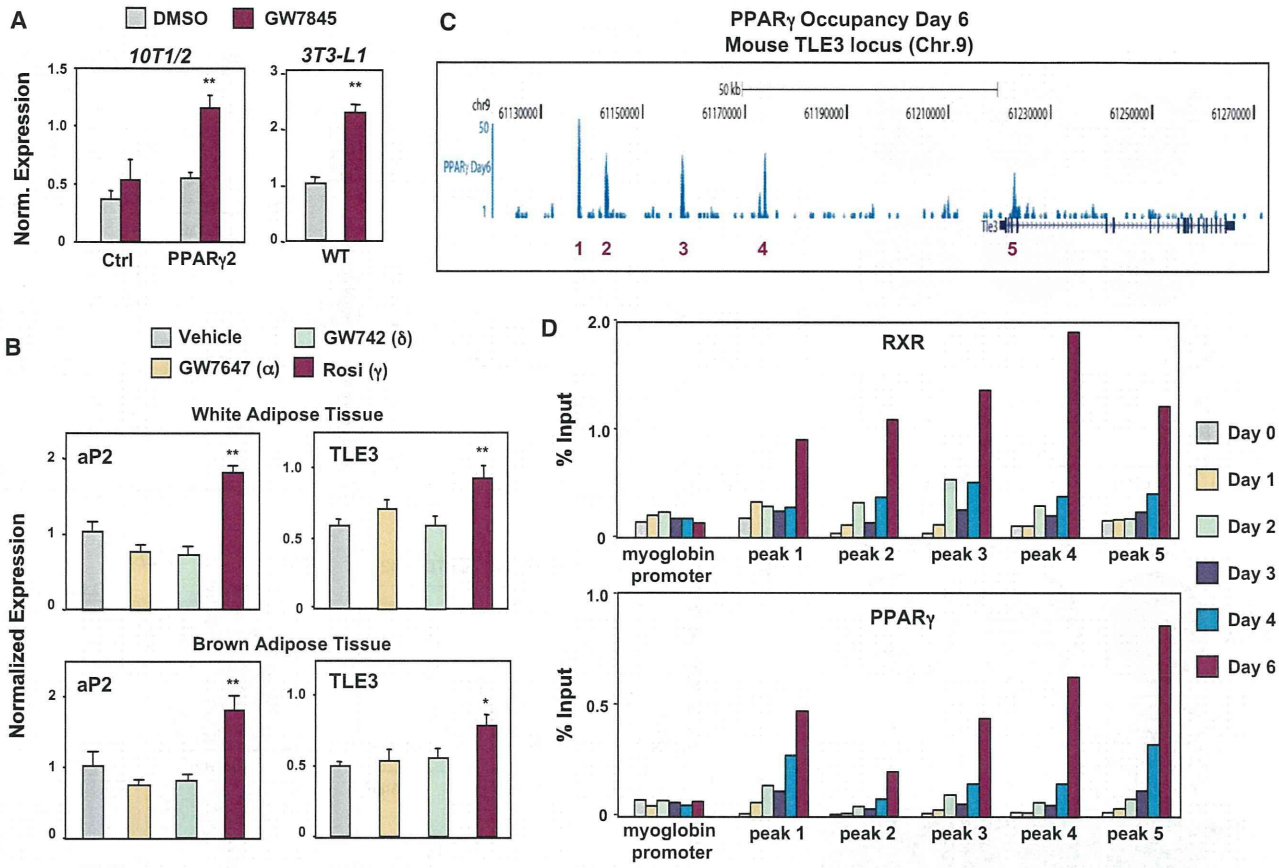

Figure 2. TLE3 Is a PPARγ Target Gene

(A) Real-time PCR analysis of TLE mRNA expression in PPARγ2-expressing 10T1/2 preadipocytes treated with 100 nM GW7845 for 2 days (left) and 3T3-L1 preadipocytes treated with DMI + 20 nM GW for 2 days (right).

(B) Induction of TLE3 and aP2 mRNA by PPARγ agonist in white and brown adipose tissue in vivo. Mice were gavaged twice daily for 2 days with vehicle, PPARα agonist (10 mg/kg GW7647), PPARδ agonist (10 mg/kg GW742), or PPARγ agonist (30 mg/kg rosiglitazone). Male mice, N = 10 per group, $^{*}p < 0.05$, $^{**}p < 0.01$.

(C) High-resolution ChIP-Seq analysis of PPARγ binding sites within the mouse TLE3 locus from 3T3-L1 cells differentiated for 6 days with DMI. These data are from the deep sequencing study of Nielsen et al., 2008.

(D) Differentiation-dependent PPARγ/RXR occupancy in the vicinity of the TLE3 gene. ChIP of PPARγ and RXR in 3T3-L1 cells was followed by qPCR analysis using primers flanking individual PPARγ binding sites in the TLE3 gene region at the indicated time points. A region of the myoglobin promoter served as a negative control. Error bars represent mean ± SD. See also Figure S2.

expression of PPARγ and many of its downstream target genes in cells stably expressing TLE3 (Figures 3B, S3A, and S3B).

We turned to the NIH 3T3 fibroblast system to investigate potential combinatorial effects of TLE3 and PPARγ. NIH 3T3 cells are unable to differentiate into adipocytes because they lack PPARγ. Expression of TLE3 in this context had little if any effect on the expression of PPARγ target genes (Figures 3C and S3C). Consistent with prior work (Tontonoz et al., 1994c), introduction of PPARγ conferred the ability to accumulate lipid and express adipogenic genes (Figure 3C) (data not shown). The combination of PPARγ and TLE3 was highly synergistic, both in terms of target gene expression and morphological differentiation (Figure 3C) (data not shown). These data demonstrate that the effects of TLE3 on adipogenic gene expression are highly dependent on PPARγ expression.

In order to address whether endogenous TLE3 activity contributes to adipogenesis, we used retroviruses encoding inhibitory shRNAs to knock down TLE3 expression. TLE3 knockdown was confirmed by immunoblotting (Figure S3D). Stable 3T3-L1 cell lines expressing two different shRNA sequences targeting TLE3 exhibited reduced differentiation capacity, compared to those expressing a control shRNA (Figure 3D). In agreement with the morphological differentiation, the expression of adipocyte-selective genes was also impaired in TLE3 knockdown cells (Figures 3E and S3E).

As a complement to the knockdown studies, we generated mice lacking TLE3 using a Gene Trap embryonic stem cell line obtained from The Sanger Centre (XP0165), in which the insertion of the trapping vector resulted in a null allele. Unfortunately, homozygous deletion of TLE3 results in embryonic lethality due to multiple developmental defects (data not shown). However, we succeeded in deriving primary MEFs from TLE3−/− mice. Multiple preparations of primary embryonic fibroblasts derived from TLE3−/− mice showed reduced capacity for adipogenesis, compared to WT controls (Figure 3F). Adipogenic gene expression was correspondingly reduced in MEFs lacking TLE3

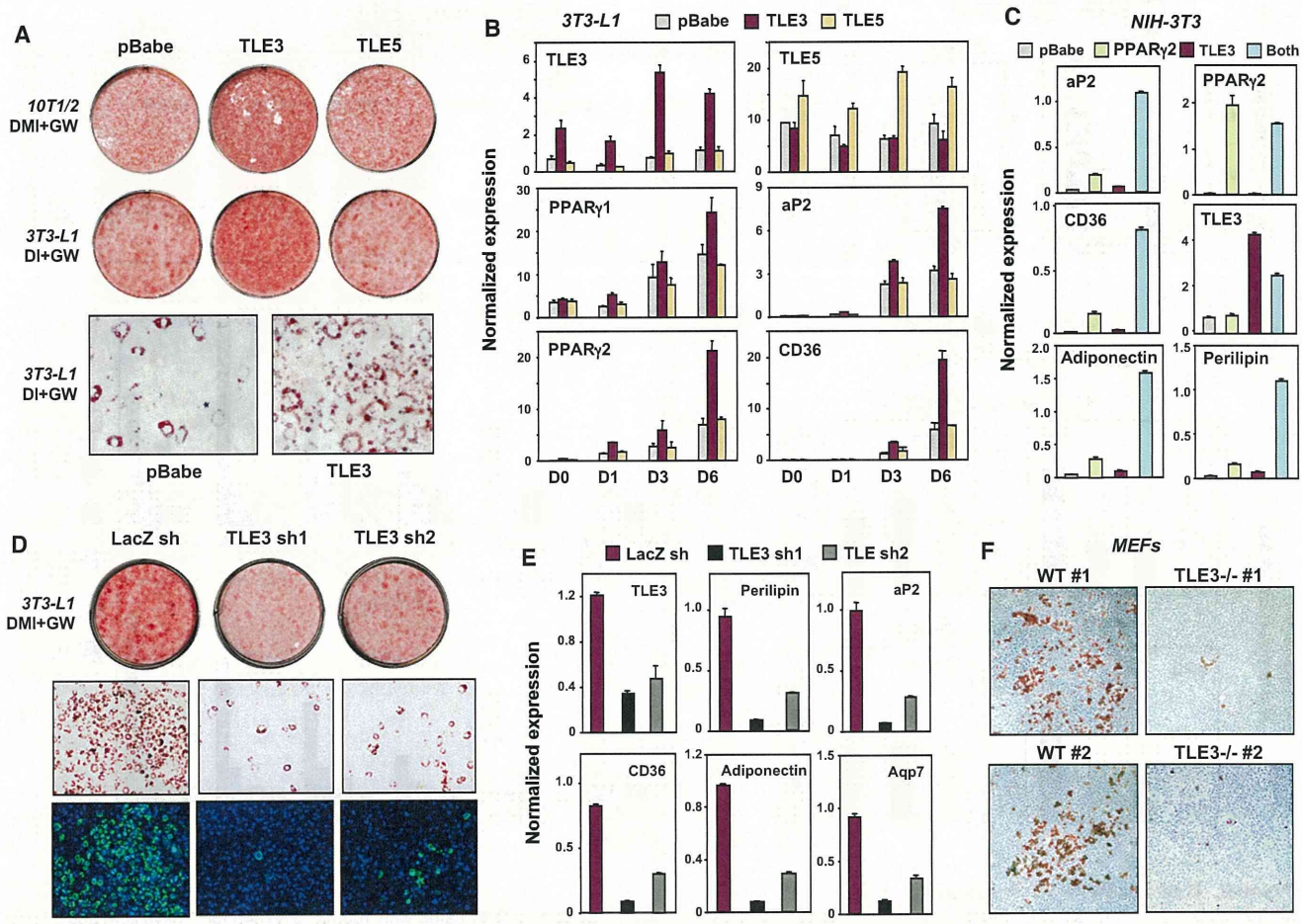

Figure 3. TLE3 Is a Transcriptional Modulator of Adipogenesis

(A) Analysis of differentiation by oil red O (ORO)-staining of retrovirally derived stable 10T1/2 and 3T3-L1 cell lines expressing vector TLE3 or TLE5. 10T1/2 and 3T3-L1 cells were stimulated to differentiate with DMI + 20 nM GW for 7 days and 10 days, respectively. Top: plate view of ORO-stained cultures; bottom: microscopic view.

(B) Real-time PCR analysis of adipogenic gene expression in 3T3-L1 cells transduced with TLE3 or TLE5.

(C) NIH 3T3 cells stably expressing TLE3, PPARγ, or both from retroviral vectors were stimulated to differentiate with dexamethasone (2 μM), insulin (5 μg/ml), and GW7845 (20 nM) for 10 days.

(D) Adipogenic potential of 3T3-L1 cells expressing lentivirally delivered shRNAs targeting TLE3 or lacZ shRNA control. Infected 3T3-L1 cells were stimulated to differentiate with DMI + 10 nM GW for 7 days. Top: plate view of ORO-stained cultures; middle: microscopic view; bottom: microscopic view of BODIPY (lipid)- and DAPI (nuclei)-stained cells.

(E) Expression of PPARγ target genes in 3T3-L1 cells expressing TLE3 shRNAs as determined by real-time PCR. Cells were treated with DMI + GW (10 nM) for 7 days. Error bars represent mean ± SD.

(F) Adipogenic potential of individually derived primary WT or TLE3 null mouse embryonic fibroblasts (MEFs). Cells were stained with ORO after stimulation with DMI + 1 μM rosiglitazone for 6 days, followed by 6 days with rosiglitazone and insulin. See also Figure S3.

(Figure S3F). Together, these data demonstrate that TLE3 is a physiologic component of the adipogenic program that works cooperatively with PPARγ to promote differentiation.

TLE3 Facilitates PPARγ-Dependent Gene Activation

Next we addressed the mechanism of TLE3 action in adipogenesis. As chronic (stable) overexpression of TLE3 was able to induce expression of PPARγ, aP2, and CD36 in undifferentiated 10T1/2 cells, it was possible that TLE3 was functioning primarily by inducing PPARγ expression, leading to secondary effects on downstream target genes. To address whether acute expression of TLE3 could also induce adipogenic gene expression, we transduced 10T1/2 cells expressing the coxsackie adenovirus receptor (CAR) with an adenoviral vector encoding TLE3. Surprisingly, TLE3-tranduced cells showed increased expression of aP2 and CD36 and enhanced response to PPARγ agonist, despite expressing similar endogenous levels of both PPARγ1 and PPARγ2 (Figure 4A) (data not shown). These effects occurred in the absence of morphological differentiation. Many PPARγ target genes are also regulated by C/EBPs; however, the expression of C/EBPs was also not altered by TLE3 (Figure S4A). The ability of TLE3 to regulate target genes without affecting PPARγ expression suggested that TLE3 might be enhancing PPARγ activity. We further explored this possibility

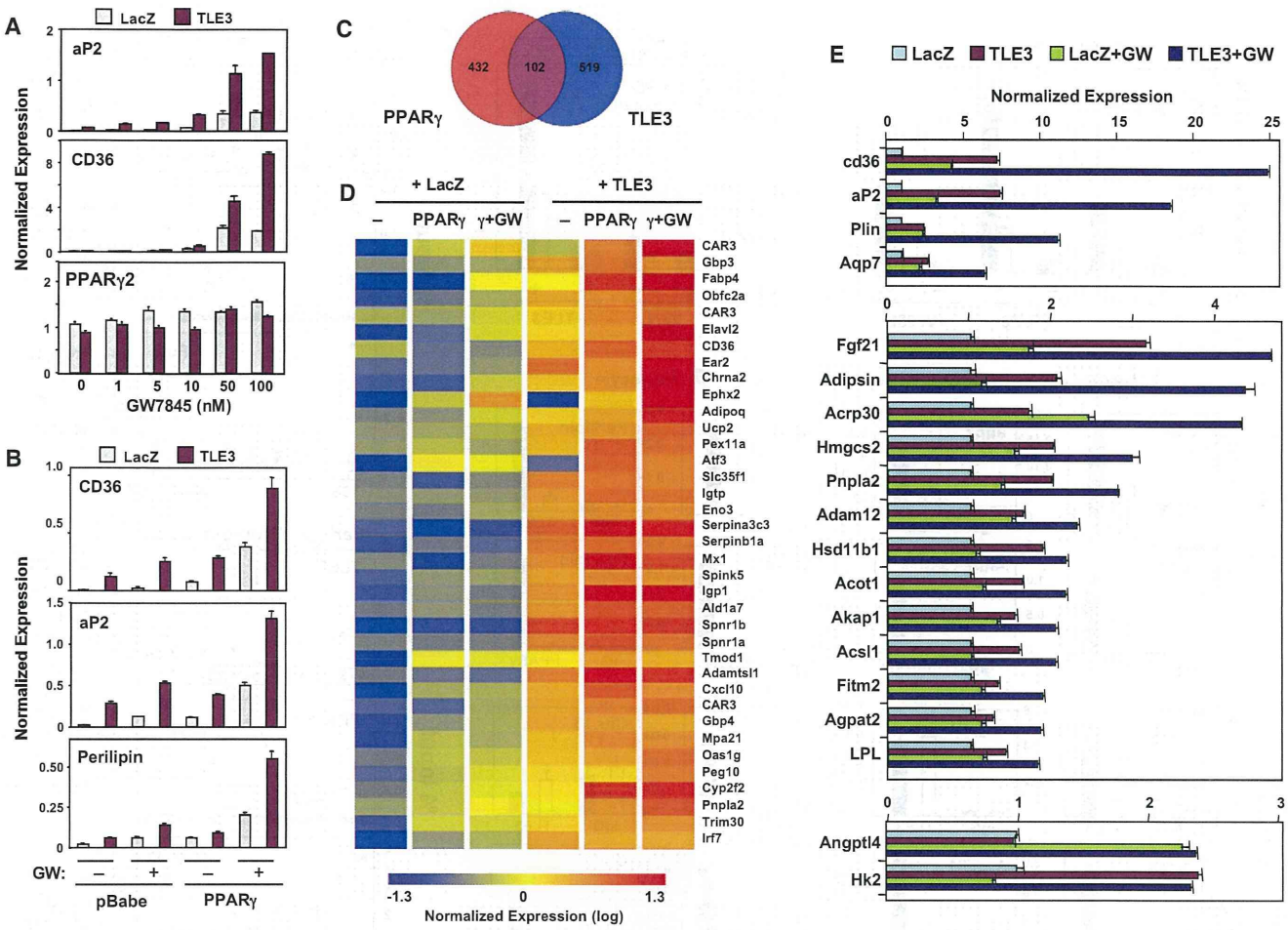

Figure 4. Overlapping Transcriptional Profiles of PPARγ- and TLE3-Regulated Genes

(A) Confluent 10T1/2 cells expressing the coxsackie adenovirus receptor (CAR) were infected with lacZ- or TLE3-expressing adenoviruses and simultaneously treated with GW7845 at the indicated concentrations for 48 hr. Gene expression was determined by real-time PCR.

(B) Effects of TLE3 expression on adipogenic genes are dependent on the level of PPARγ expression. Postconfluent 10T1/2 CAR cells stably expressing vector (pBabe) or PPARγ2 were infected overnight with lacZ- or TLE3-expressing adenovirus. Forty-eight hours postinfection, cells were treated with DMSO or 10 nM GW7845.

(C) Venn diagram of overlapping transcriptional programs of PPARγ and TLE3 in 10T1/2 cells.

(D) Heatmap representation of selected PPARγ- and TLE3-responsive genes (>1.4 change) identified by analysis of Affymetrix arrays.

(E) Validation of gene expression changes from microarray analysis by real-time PCR. PPARγ-expressing 10T1/2 cells infected with lacZ or TLE3 adenovirus were treated with DMSO or 10 nM GW7845 for 24 hr. Error bars represent mean ± SD. See also Figure S4.

by acutely expressing TLE3 in the presence of stably expressed PPARγ. As shown in Figure 4B, TLE3 strongly promoted the ability of PPARγ to induce its target genes in response to agonist. These data suggest that the primary effect of TLE3 is on PPARγ activity and that the elevated level of PPARγ observed in cells stably expressing TLE3 is secondary to increased adipocyte differentiation.

We next employed transcriptional profiling to compare the PPARγ and TLE3 transcriptomes. We acutely expressed TLE3 and PPARγ individually and in combination in 10T1/2 cells by viral transduction. Gene expression was analyzed after 48 hr using Affymetrix Mouse Gene 1.0 ST Arrays. Despite previous characterization of TLEs as repressors, a greater number of transcripts were induced in response to TLE3 expression than suppressed (Figure S4B). Furthermore, the transcriptional programs engaged by TLE3 and PPARγ were highly overlapping, as indicated by the Venn diagram in Figure 4C. Approximately 25% of PPARγ-responsive genes overlapped with those regulated by TLE3, indicating a significant degree of specificity for the PPARγ transcriptional program. Cluster analysis of the entire set of overlapping genes is presented in Figure S4C and Tables S1 and S2. A more limited set of genes, whose expression was altered more than 1.4-fold, is presented in Figure 4D. Importantly, the common regulated genes identified in this analysis included many established PPARγ targets, including aP2, CD36, and adiponectin (Figure 4D). Furthermore, it is clear from the heat map of Figure 4D that PPARγ and TLE3 have additive or synergistic effects on the expression of a large battery of genes. In agreement with the additive effects of these factors in adipogenesis (Figure 3C), maximal expression of this

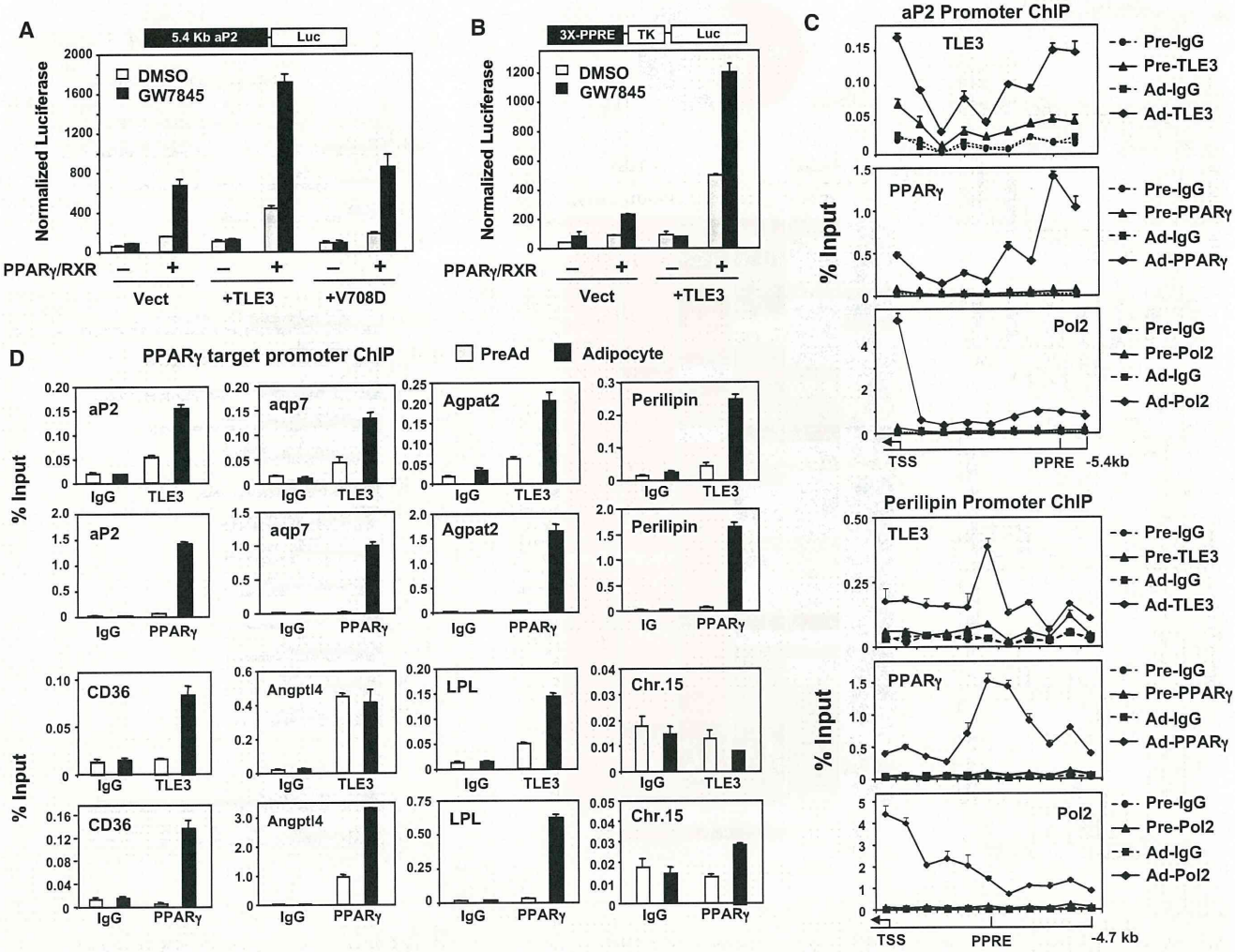

Figure 5. TLE3 Coactivates PPARγ-Dependent Gene Expression

(A) Analysis of −5.4 kb aP2 enhancer activation by coexpression of PPARγ/RXR and TLE3 or TLE3 carrying a mutation in the WD40 (V708D) domain in undifferentiated 10T1/2 cells treated with DMSO or 100 nM GW7845.

(B) TLE3 enhances PPARγ/RXR activation of a luciferase reporter driven by minimal PPAR-responsive elements (3X-PPRE). Cells were treated as in (A).

(C) Differentiation-dependent recruitment of TLE3 to the endogenous aP2 and perilipin promoters in 10T1/2 cells. ChIP assays were carried out using TLE3, PPARγ, RNA Pol2, and control IgG in preadipocytes (Pre) and adipocytes (day 6 DMI + 20 nM GW; Ad). Individual regions of the aP2 and perilipin upstream regions from the (TSS) to 5.4 kb upstream and 4.7 kb upstream were amplified by real-time PCR, respectively.

(D) ChIP analysis of TLE3 recruitment to the PPREs of PPARγ target gene promoters in differentiated adipocytes. A nonspecific region in Chr. 15 was used as a control. ChIP signals were quantified by real-time PCR. Error bars represent mean ± SD. See also Figure S5.

gene set was achieved in the presence of TLE3, PPARγ, and GW7845 (Figure 4D). Our global transcriptional analysis did not reveal a significant effect of TLE3 expression on the programs of other nuclear receptors, including LXR, FXR, or RAR (data not shown).

We validated our array results for a number of direct PPARγ targets by real-time PCR analysis (Figure 4E). The results confirmed that the vast majority of established direct PPARγ target genes in adipocytes were additively responsive to TLE3 and PPARγ. For some genes, such as aP2 and perilipin, the response was synergistic. A minority of putative PPARγ target genes was responsive to PPARγ but not TLE3 (e.g., Angptl4) or TLE3 but not PPARγ (e.g., HK2) (Figure 4E).

Differentiation-Dependent Recruitment of TLE3 to PPREs

The ability of TLE3 to selectively promote PPARγ-dependent target gene expression suggested that TLE might function as a positive transcriptional cofactor for PPARγ. To test this idea, we performed transfection assays with a −5.4 kb aP2-luciferase reporter. 10T1/2 cells transfected with PPARγ and RXR expression vectors showed robust luciferase activity in the presence of GW7845 (Figure 5A). TLE3 had no effect in the absence of PPARγ and RXR, but enhanced reporter activity when these nuclear receptors were present. Introduction of the point mutation in the WD40 domain of TLE3 (V708D) that prevented TLE from inducing adipogenesis also prevented coactivation

of PPARγ (Figure 5A). TLE3 showed similar ability to enhance PPARγ-dependent transcription when a reporter driven by isolated PPAR response elements (PPREs) was used (Figure 5B). This result strongly suggested that TLE3 was acting to increase aP2-promoter transcription by increasing PPARγ activity on its cognate response element, rather than by acting through other binding sites. Preliminary studies indicated that TLE3 also promoted the action of PPARα and PPARδ in transfection assays (Figure S5A).

To provide additional evidence for the ability of TLE3 to enhance PPARγ activity on PPREs, we performed ChIP assays in 10T1/2 cells. We initially analyzed PPARγ and TLE3 occupancy along the 5′-flanking region of the aP2 gene extending from −5.4 kb to the transcriptional start site. Strong differentiation-dependent binding of PPARγ was detected in the region corresponding to the previously characterized PPREs in the aP2 enhancer (Tontonoz et al., 1994a). Remarkably, TLE3 was also found to occupy the aP2 promoter/enhancer in a differentiation-dependent manner (Figures 5C and 5D). A strong peak was detected in the region corresponding to the PPREs, coincident with PPARγ binding, and an additional peak was noted closer to the proximal promoter. As expected, Pol2 occupancy was detected at the transcriptional start site in adipocytes but not preadipocytes. Analysis of the 5′-flanking region of the perilipin gene revealed similar differentiation-dependent co-occupancy of PPARγ and TLE3 in the region of the PPRE (Figure 5C).

We next addressed whether TLE3 was localized with PPARγ on the regulatory regions of other adipocyte PPARγ target genes. Indeed, regulatory regions containing previously validated PPREs from the CD36, Aqp7, Agpat2, LPL, and perilipin genes were all co-occupied by PPARγ and TLE3 in a differentiation-dependent manner (Figure 5D). By contrast, there was no enrichment of PPARγ or TLE3 on control regions not containing PPREs, such as a sequence on Chromosome 15 (Figure 5D). Interestingly, we did not observe differentiation-dependent changes in TLE3 occupancy on the Angptl4 promoter. This finding was consistent with our prior observation that TLE3 expression did not enhance Angptl4 expression (Figure 4E).

We also investigated whether TLE3 could be localized to PPARγ-containing complexes in adipocytes. We were unable to detect a direct interaction between TLE3 and PPARγ using standard in vitro pull-down assays (data not shown). However, two different lines of evidence support the hypothesis that these proteins are present in a transcriptional complex. First, TLE3 could be identified in complexes immunoprecipitated from 10T1/2 adipocytes with a PPARγ antibody (Figure S5B). Second, TLE3 was independently identified as a PPARγ-associated protein in mass spectrometry analysis of PPARγ-containing fractions purified from 3T3-L1 adipocytes (R.N. and S.M., unpublished data). Together, these data indicate that TLE3 is present in PPARγ-containing differentiation-dependent transcriptional complexes and facilitates adipocyte differentiation by enhancing the activity of PPARγ on its target promoters.

TLE3 Counteracts Wnt Signaling in Preadipocytes

Studies in *Drosophila* have characterized the TLE ortholog groucho as a repressor that binds TCF and inhibits Wnt signaling (Cavallo et al., 1998). We hypothesized that increased TLE3 expression during differentiation might provide a mechanism for counteracting Wnt signaling in this context. In support of this idea, we found that TLE3 could be identified in complexes immunoprecipitated from 3T3-L1 adipocytes with a TCF4 antibody (Figure S5B). Furthermore, the expression of Wisp2, a Wnt-responsive gene highly expressed in preadipocytes, was strongly downregulated during adipogenesis, coincident with upregulation of TLE3 (Figure 6A). We observed substantial increases in TLE3 protein levels 2 days following stimulation of preadipocytes with differentiation cocktail, and this correlated with the time course of Wnt target gene decline. In fact, TLE3 protein expression was more highly regulated during differentiation, compared to the expression of either TCF4 or β-catenin (Figure 6B).

This led us to propose that TLE3 may antagonize β-catenin binding to TCF during differentiation and thereby inhibit TCF action. To test this possibility, we expressed TLE3 in preadipocytes and then challenged cells with control or Wnt-conditioned media. TLE3 blunted the induction of both Nkd2 and Wisp2 upon Wnt activation in 10T1/2 cells (Figure 6C). A similar result was observed in undifferentiated 3T3-L1 cells for Axin2 and Nkd2 (Figure 6C). We also found that TLE3 expression could counteract the repressive action of Wnt3a on adipogenic genes, including aP2, CD36, and, to a lesser degree, PPARγ (Figure 6D).

To test whether TLE3 could directly inhibit Wnt-dependent transcription, we performed transient transfection assays using the Wnt-responsive TOPflash reporter (3X LEF1). Cotransfection of a TLE3 expression vector antagonized the ability of β-catenin to activate the TOPflash reporter. Similarly, TLE3 expression blocked activation of the TOPflash reporter in cells stimulated with LiCl, a potent inhibitor of GSK3β and activator of TCF-dependent transcription (Figure 6E).

Although the ability of β-catenin and TCF to inhibit adipogenesis is well documented, the mechanisms involved are poorly understood. Recent studies in other systems have shown that β-catenin can act as a repressor of transcription through a TCF/Lef1-dependent mechanism (Blauwkamp et al., 2008). We hypothesized that TCF-β-catenin complexes might be exerting repressive effects directly at the promoters of adipogenic genes. Remarkably, we found, using ChIP, that TCF and β-catenin colocalized along the −5.4 kb aP2 promoter/enhancer in undifferentiated cells (Figures S6 and 6F). This occupancy decreased upon differentiation into adipocytes, consistent with Wnt signaling diminishing over the course of differentiation (Figure 6F). Interestingly, treatment of preadipocytes with Wnt3a-conditioned media increased β-catenin occupancy, but TCF4 occupancy remained constant. Thus, recruitment of β-catenin was associated with repression of the aP2 promoter in undifferentiated cells. Furthermore, the presence of β-catenin was inversely correlated with the presence of TLE3 (Figure 6F).

To address the effect of TLE3 on recruitment of β-catenin, we used adenoviral vectors to express TLE3 in undifferentiated cells. ChIP assays demonstrated that TLE3 strongly inhibited β-catenin occupancy of the aP2 promoter, both in the presence and absence of exogenous Wnt (Figure 6G). Together, our observations suggest that increased TLE3 expression during adipogenesis promotes differentiation by two related mechanisms. First, it binds together with PPARγ to adipocyte gene promoters and facilitates PPARγ-dependent activation. Second, TLE3 forms complexes with TCFs that fail to recruit β-catenin, thus relieving the repression of adipocyte promoters.

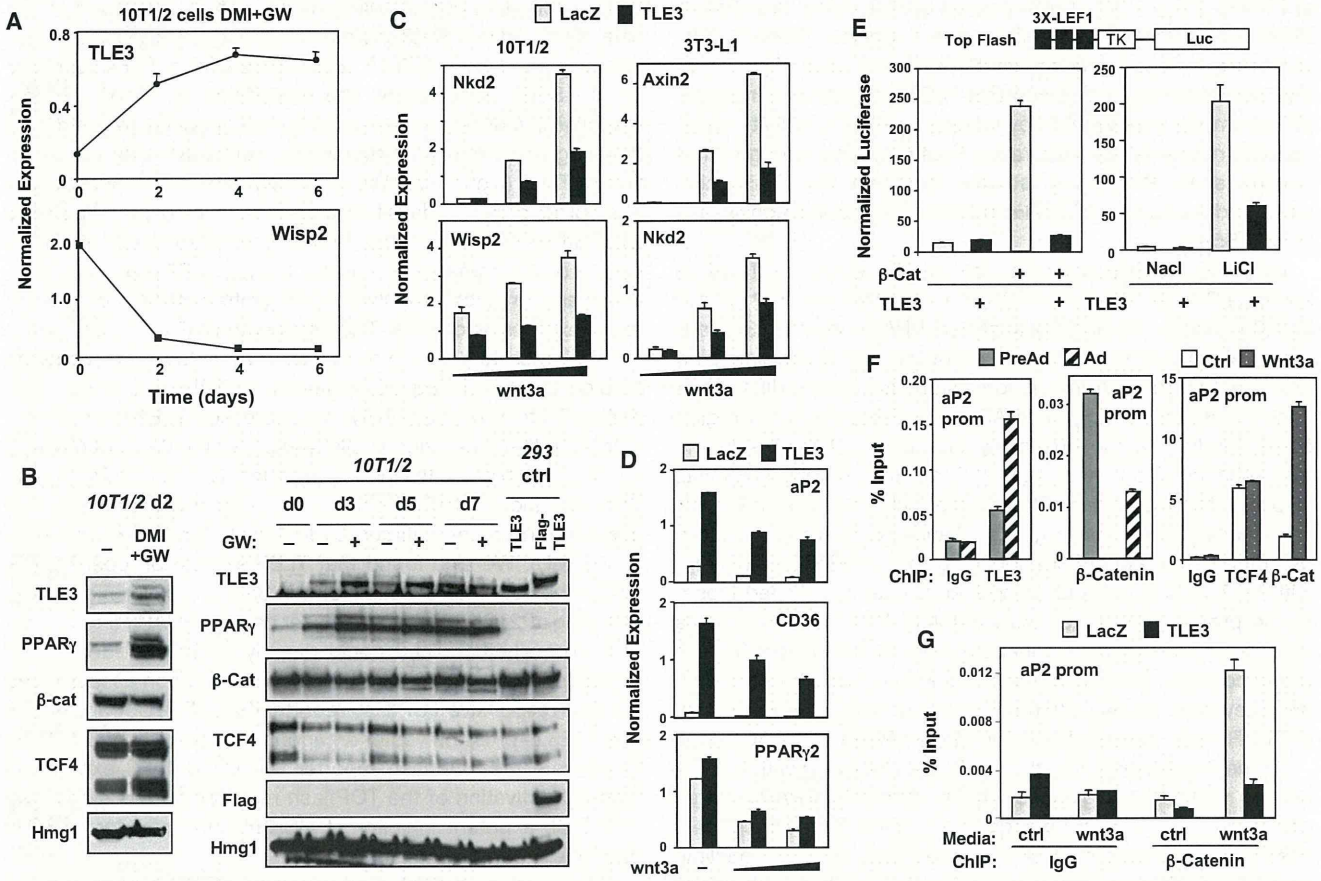

Figure 6. TLE3 Counteracts Wnt Repression of Adipocyte Promoters through Corepression of TCF4

(A) Real-time PCR analysis of mRNA expression in 10T1/2 cells induced to differentiate with DMI and GW7845.

(B) Immunoblot analysis of 10T1/2 cells stimulated to differentiate with DMI ± 20 nM GW as indicated.

(C) Undifferentiated 10T1/2 and 3T3-L1 cells stably expressing CAR were infected with lacZ or TLE3 adenovirus overnight. Cells were treated 2 days postinfection with control or Wnt3a-conditioned media for 24 hr. Gene expression was determined by real-time PCR.

(D) 10T1/2 cells were transduced with control or TLE3 adenovirus vectors and treated for 24 hr with Wnt-conditioned media. Gene expression was determined by real-time PCR.

(E) Effect of TLE3 transfection on activation of the Wnt-responsive TOPflash reporter by β-catenin (left) and GSK3β inhibitor LiCl (25 mM for 24 hr) (right) in 293T cells.

(F) Reciprocal occupancy of β-catenin and TLE3 on the aP2 promoter. ChIP assays of aP2 promoter binding were carried out for TLE3, TCF4, and β-catenin in preadipocytes (Pre-Ad) and adipocytes (Ad).

(G) 10T/12 cells stably expressing CAR were infected overnight with lacZ or TLE3 adenovirus. Forty-eight hours postinfection, cells were treated with control or Wtn3a-conditioned media for 24 hr. ChIP assays were carried out using control IgG and β-catenin antibodies. Note: the data for TLE3 in (A) and (B) are the same as shown in Figure 1 and are included here for comparison. Error bars represent mean ± SD. See also Figure S6.

Expression of TLE3 in Adipose Tissue Mimics PPARγ Activation

Because our studies indicated that TLE3 selectively promoted the PPARγ transcriptional program in cultured cells, we investigated its activity in adipose tissue in vivo. We generated transgenic mice expressing human TLE3 in adipose tissue using the −5.4 kb aP2 promoter/enhancer (Figure 7A). Adipose-selective expression of transgenic TLE3 was confirmed using qPCR primers specific for human TLE3 (Figure 7A). Immunoblot analysis revealed modestly increased TLE3 protein levels in WAT and BAT from aP2-TLE3 mice (Figures 7A and S7A). DEXA analysis revealed a trend toward increased fat mass, but no differences in total body weight, bone mineral density, or lean body mass between WT and aP2-TLE3 mice (Table S3). However, aP2-TLE3 mice fed a high-fat diet for 10 weeks exhibited increased epididymal WAT mass when compared to WT littermates (Figure 7B). By contrast, liver mass was slightly reduced when corrected for body weight. Furthermore, real-time PCR analysis demonstrated that expression of the PPARγ target genes aP2 and CD36 was modestly elevated in WAT from aP2-TLE3 mice (Figure 7C). Notably, the magnitude of these changes was consistent with the expected effect of synthetic PPARγ agonist (Figure 2B). Plasma levels of the PPARγ-responsive adipokines adiponectin and resistin were also found to be elevated in aP2-TLE3 mice (Figure 7D). However, plasma leptin levels were not different between groups. The lack of a change in leptin levels despite increased fat mass is consistent with prior reports that PPARγ ligands suppress leptin expression (De Vos et al., 1996).

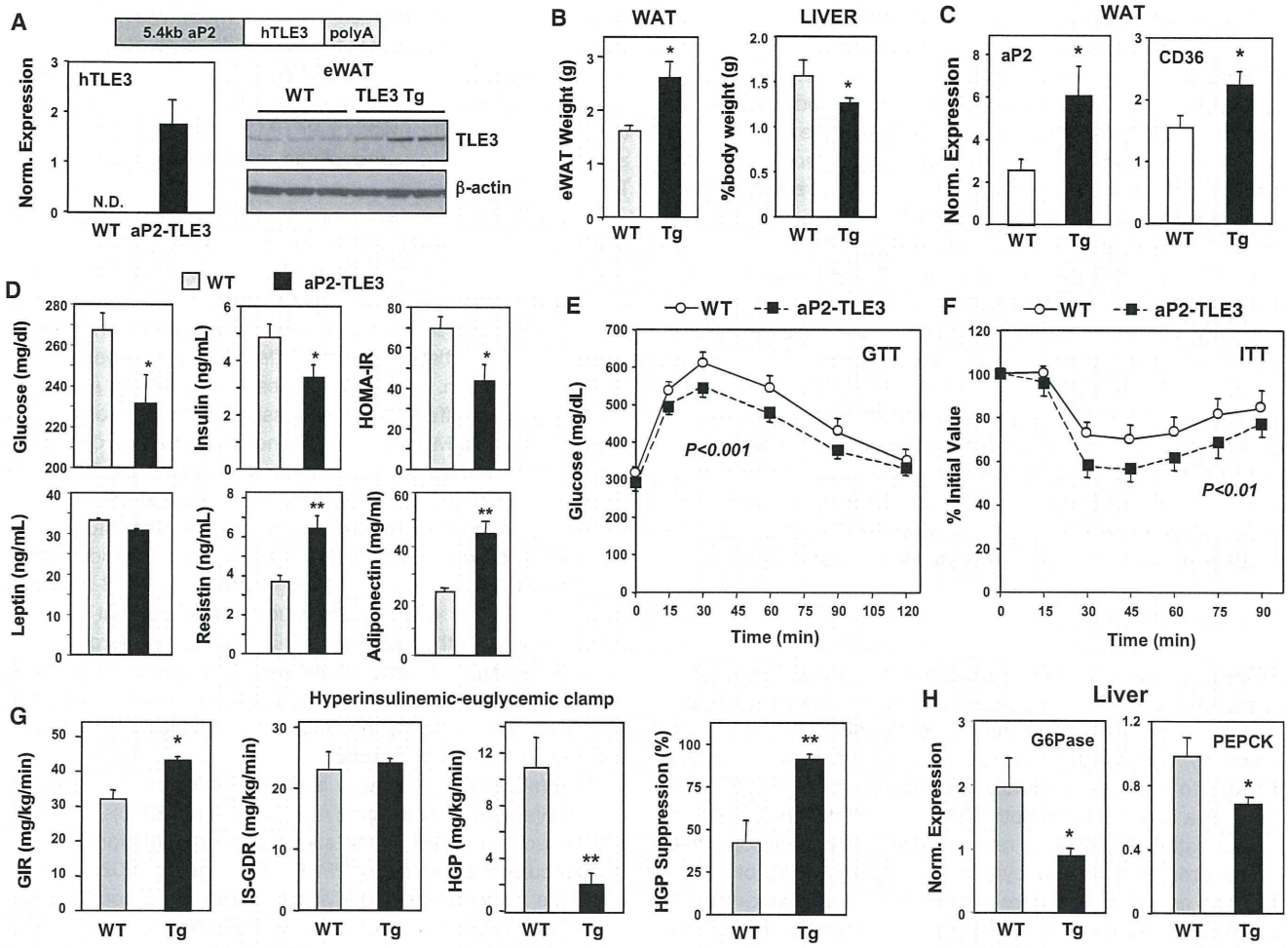

Figure 7. Transgenic Expression of TLE3 in Adipose Tissue Ameliorates Insulin Resistance

(A) Expression of TLE3 in epididymal WAT of aP2-TLE3 transgenic mice. Left: real-time PCR analysis of human TLE3 transcript; right: immunoblot analysis of TLE3 and β-actin. Chow-fed C57BL/6 male mice, N = 3 per group.

(B) Weight of eWAT and liver percent of body mass in high-fat-fed WT and aP2-TLE3 (Tg) transgenic mice. 14 weeks HF diet, N = 6 per group, *p < 0.05.

(C) Real-time PCR analysis of aP2 and CD36 expression in eWAT from 14 weeks HF-fed mice. N = 5–6 per group, *p < 0.05.

(D) Plasma glucose, insulin, leptin, resistin, and adiponectin levels from mice fed high-fat diet for 11 weeks. Homeostatic model assessment insulin resistance (HOMA-IR) index was computed from glucose and insulin values. 6 hr fasting, N = 5–6 per group, *p < 0.05.

(E and F) Glucose tolerance test (GTT) and insulin tolerance test (ITT) were performed after 6 weeks and 9 weeks of HF diet, respectively. N = 5–6 per group. P values were determined by two-way ANOVA followed by Bonferroni post hoc test.

(G) Improved insulin sensitivity and reduced hepatic glucose production in aP2-TLE3 transgenic mice. Glucose infusion rate (GIR), insulin-stimulated glucose disposal (IS-GDR), and hepatic glucose production (HGP) were determined by hyperinsulinemic euglycemic clamp studies of 14 weeks HF-fed WT mice and aP2-TLE3 mice. N = 5–6 per group, *p < 0.05, **p < 0.01.

(H) Reduced expression of the gluconeogenic enzymes glucose-6-phosphatase (G-6-Pase) and PEPCK determined by real-time PCR analysis of livers from 14 weeks HF-fed mice. N = 5–6 per group, *p < 0.05. Error bars represent mean ± SD. See also Figure S7.

Elevated adiponectin levels often coincide with improved insulin sensitivity. We therefore investigated whether adipose tissue expression of TLE3 would impact glucose homeostasis in the context of diet-induced obesity. Compared to WT controls, aP2-TLE3 mice fed a high-fat diet for 8 weeks showed reduced fasting (6 hr) glucose, insulin, and homeostatic model assessment insulin resistance (HOMA-IR) index (Figure 7D). All of these parameters are indicative of improved glucose homeostasis. To further confirm this, we performed glucose and insulin tolerance tests (GTT, ITT). Adipose TLE3 expression was associated with both increased glucose tolerance and increased insulin sensitivity (Figure 7F). A trend toward improved glucose homeostasis was observed in a second line of transgenic mice (aP2-TLE3B) that exhibited lower TLE3 expression (Figure S7B). We did not observe a difference in glucose tolerance between aP2-TLE3 and WT mice fed a normal chow diet (Figure S7C). Metabolic cage analysis revealed modest but significant reduction in energy expenditure in Tg compared to WT mice (Figure S7D). Thus, although the aP2-TLE3 transgene is also expressed in BAT, these data suggest that the improvement in glucose homeostasis is unlikely to be due to enhanced fatty acid oxidation in BAT. Food intake was also reduced in aP2-TLE3 mice compared to WT.

Finally, we performed hyperinsulinemic-euglycemic clamp studies in order to more directly measure insulin sensitivity and gain insight into the tissues involved in the phenotype of aP2-TLE3 mice. aP2-TLE3 mice required an increased glucose infusion rate (GIR) to maintain euglycemia, a sensitive measurement of whole-body insulin sensitivity (Figure 7G). Insulin-stimulated glucose disposal rate (IS-GDR), which primarily reflects skeletal muscle insulin sensitivity, was similar between genotypes (Figure 7G). By contrast, the suppression of hepatic glucose production (HGP) by insulin was improved in aP2-TLE3 mice relative to controls. These findings indicate that the observed changes in GIR largely reflected improved hepatic insulin sensitivity. Histological analysis of livers revealed that aP2-TLE3 mice had reduced lipid accumulation in the liver (Figure S7E). The expression of gluconeogenic genes was reduced in aP2-TLE3 mice in accordance with the HGP results (Figure 7H). Interestingly, a selective effect on HGP compared to IS-GDR is consistent with the effect of low-dose TZD administration (Kubota et al., 2006). Thus, our results are in line with the expected effects of modest stimulation of the adipocyte PPARγ pathway.

DISCUSSION

Here we outline a role for a member of the highly conserved groucho transcription factor family as a facilitator of nuclear receptor action during cell differentiation. TLE3 is a direct target for regulation by PPARγ and functions in a feed-forward loop with PPARγ to promote differentiation. Mechanistically, TLE3 functions as a coregulator of both PPARγ and Wnt signaling, driving the formation of active and repressive transcriptional complexes on the promoters of adipocyte genes. The dual ability of TLE3 to function as a coactivator for PPARγ and a corepressor for TCF provides an elegant mechanism for the integration of pro- and antiadipogenic signals during adipocyte development.

The function of TLE proteins in adipocyte development has not previously been investigated. Our discovery of TLE3 as a coactivator for PPARγ-dependent transcription was unexpected, as groucho and mammalian TLEs have been primarily studied for their roles as corepressors (Chen and Courey, 2000). TLE proteins lack a DNA-binding domain, and therefore their ability to regulate transcription is believed to be dependent on interaction with other proteins. Several transcription factors are known to interact with TLEs, including PAX, Hes, Engrailed, and TCFs (Buscarlet and Stifani, 2007). TLEs are recruited to silence gene expression in various contexts through direct interactions with histones and histone-modifying enzymes (Chen et al., 1999; Sekiya and Zaret, 2007). Our demonstration that TLE3 expression acts to positively reinforce PPARγ action has uncovered a previously unrecognized mode of action for this transcriptional cofactor.

Previous work has identified several coactivators that interact with PPARγ (Cho et al., 2009; Ge et al., 2002; Gelman et al., 1999; Grøntved et al., 2010; Louet et al., 2006; Qi et al., 2003; Takahashi et al., 2002). Unlike TLE3, however, the levels of these factors are not regulated during differentiation. They are likely required for the efficient action of PPARγ and other transcription factors, but are not utilized as developmental switches per se. PGC-1α, a coregulator whose expression is highly regulated by physiological stimuli, is critical for the brown adipocyte thermogenic program, but is not believed to play a central role in white adipose differentiation (Puigserver et al., 1998). The high expression of TLE3 in WAT, relative to BAT, leads us to speculate that TLE3 may function as a white adipocyte counterpart to PGC-1α in brown adipocytes. Transcriptional profiling supports this, as the brown adipocyte markers PRDM16, Cidea, Elovl3, Ucp1, and PGC-1α were not upregulated in 10T1/2 cells expressing TLE3.

TLE3 mRNA and protein expression accumulate during preadipocyte differentiation and in response to PPARγ activation. Thus, coactivation of PPARγ by TLE3 may serve as a feed-forward mechanism to enhance differentiation. Expression of TLE3 at levels present in differentiated adipocytes promotes preadipocyte differentiation, and this effect is highly dependent on PPARγ expression. Indeed, coexpression of PPARγ and TLE3 has a synergistic effect on the expression of a number of terminal adipocyte genes. Moreover, we found a high degree of overlap between the transcriptional programs regulated by TLE3 and PPARγ, indicating that TLE3 exerts a preferential effect on the PPARγ signaling pathway in this cell type. Further studies will be needed to determine whether there may be additional transcription factors other than PPARγ involved in TLE3 signaling in preadipocytes. Mechanistic studies indicate that TLE3 is recruited along with PPARγ to PPREs in adipocyte target genes in a differentiation-dependent manner. PPARγ and TLE3 can be localized to common transcription complexes by immunoprecipitation and biochemical purification, although the two proteins do not appear to interact directly.

The Wnt signaling pathway is important for the maintenance and proliferation of preadipocytes (Ross et al., 2000). Differentiation is accompanied by the suppression of Wnt signaling and the concurrent activation of PPARγ (Ross et al., 2002). Surprisingly, the mechanisms underlying this switch are poorly understood. In particular, it is unclear how the Wnt pathway is shut off. We propose that induction of TLE3 expression is a component of a developmental switch that silences Wnt signaling and allows adipogenesis to proceed. TCF4 and β-catenin are present on the aP2 promoter in preadipocytes, and this correlates with the suppression of transcription. In the course of differentiation, endogenous TLE3 is recruited to differentiation-dependent adipocyte promoters, where it can interact directly with TCF4 and compete for the binding of β-catenin. Forced expression of TLE3 in preadipocytes displaces β-catenin and relieves repression of differentiation-dependent genes. Interestingly, a similar mode of TCF action has recently been proposed to operate in the context of skin differentiation (Nguyen et al., 2006). TCF3 was found to actively repress epidermal and sebaceous gland differentiation in the stem cell compartment through repression of lipid metabolism genes such as PPARγ and CD36.

There is precedence for dual-function transcriptional cofactors. It is becoming increasingly clear that the strict labels of "coactivator" and "corepressor" may not accurately reflect the complex interactions of some of these nuclear proteins. For example, in addition to coactivating TCF/Lef1, β-catenin can also act as a repressor (Blauwkamp et al., 2008). The nuclear receptor cofactor RIP140 has also been reported to perform both coactivator and corepressor functions (Debevec et al., 2007; Subramaniam et al., 1999). Furthermore, the functional roles of transcriptional coregulators may be context specific and vary with the transcriptional machinery present in a particular

cell. One possibility is that TLE3 is directing chromatin remodeling and generating a chromatin structure that facilitates PPARγ-dependent transcription.

The physiological importance of TLE3 for the adipocyte program is illustrated by the demonstration that suppression of TLE3 expression compromises preadipocyte differentiation and PPARγ target gene expression. In addition, we showed that expression of TLE3 from the adipose-selective aP2 promoter in mice mimics the effect of synthetic PPARγ agonist administration. aP2-TLE3 transgenic mice challenged with a high-fat diet were partially protected against insulin resistance. Clamp studies showed that the improvement in glucose handling in aP2-TLE3 mice was largely attributable to improved hepatic insulin sensitivity. This result is in line with previously reported effects of low-dose TZD treatment. Submaximal doses of pioglitazone have been shown to increase the GIR and suppress HGP in the absence of major effects on IS-GDR (Kubota et al., 2006).

Improvements in hepatic insulin sensitivity may reflect redistribution of triglycerides away from liver and into adipose tissue. We found that aP2-TLE3 mice have increased adipose tissue, reduced liver mass, and reduced hepatic lipid accumulation on a high-fat diet. A similar finding was reported in ob/ob animals expressing an adiponectin transgene (Kim et al., 2007). Furthermore, adiponectin has been shown to act directly on the liver to suppress gluconeogenesis (Combs et al., 2001). Therefore, our demonstration that aP2-TLE3 mice have higher plasma adiponectin levels provides a plausible mechanistic explanation for the beneficial effects of TLE3 on systemic glucose metabolism. Interestingly, despite aP2-TLE3 mice having reduced food intake, their leptin levels were not elevated, suggesting a change in leptin sensitivity. Additional studies will be needed to explore this issue. Since TLE3 and aP2 are also expressed in macrophages, it will be interesting to address the function of TLE3 in this cell type and its potential contribution to the phenotype of the aP2-TLE3 mice. Finally, given the lethality of global TLE3 deficiency, future in vivo loss-of-function studies will necessitate the generation of tissue-selective conditional deletions of TLE3.

EXPERIMENTAL PROCEDURES

Cell Culture

Confluent 10T1/2 and 3T3-L1 cells were stimulated to differentiate with DMEM containing 10% FBS, 1 μM dexamethasone, 0.5 mM isobutylmethylxanthine, and 5 μg/ml insulin for 2 days, followed by 5 μg/ml insulin alone. When specified, PPARγ agonist GW7845 or rosiglitazone was included. NIH 3T3 cells were differentiated by 2 days treatment with dexamethasone, insulin, and GW7845, followed by insulin and GW7845 alone. Stable cells expressing TLE3 (Puro), PPARγ (Hygro), or CAR (Neo) were generated using pBabe retroviral vectors (Hummasti and Tontonoz, 2006). For MEF studies, TLE3 null animals were generated from ES gene trap line XP0165 obtained from The Wellcome Trust Sanger Institute. Heterozygous animals were bred to generate E13 embryos that were used to derive fibroblasts. Adipocyte differentiation was induced by treating confluent MEFs with DMEM containing 10% FBS, 0.5 mM isobutylmethylxanthine, 1 μM dexamethasone, 5 μg/ml insulin, and 1 μM rosiglitazone for 6 days. Subsequently, cells were treated for 6 days with insulin and rosiglitazone. lacZ- or TLE3-expressing adenoviruses were generated as described (Zelcer et al., 2009). Control and Wnt3a-conditioned media were prepared using L cells (ATCC) as described (Waki et al., 2007).

Cell-Based cDNA Screen

An arrayed library of 18,292 human and mouse full-length cDNAs from the OriGene TrueClone Collection (Rockville, MD) was screened by high-throughput reverse transfection of 10T1/2 cells as described (Cho et al., 2006; Waki et al., 2007). Briefly, a 15 μl mixture of FuGENE 6 and luciferase reporter (20 ng/well) in serum-free medium was added to prespotted 384-well plates containing 62.5 ng of plasmid DNA per well. PPARγ, LIP, and GAL4-LXR were used as controls. After a 30 min incubation, 2000 cells in 20 μl of DMEM supplemented with 20% FBS were added to each well. The following day, 5 μl of differentiation-induction media containing insulin (5 μg/ml) and rosiglitazone (1 μM) were added. Plates were incubated for 4 more days, and luciferase activity was determined. Relative intensities were normalized to their respective plate median values, then normalized by log2 transformation, and mean values and standard deviations were calculated for each well from the replicate screens. These values were then reverse log2 transformed, and the ratio of "afa" (derived from means) to "mfa" (derived from standard deviations) was calculated to penalize wells for replicate quality. Each cDNA was ranked by afa score. A secondary screen was performed on a set of 96 cDNAs chosen from the top afa/mfa scores reassayed in quadruplicate, and raw luciferase values were normalized to empty vector controls.

shRNA Plasmids

TLE3 shRNA constructs were designed using BLOCK-IT RNAi designer tool (Invitrogen, Carlsbad, CA). Sense and antisense oligos were annealed and cloned into pENTR/U6 plasmid (Invitrogen). Using the LR recombinase (Invitrogen), shRNA constructs were recombined into a gateway adapted pBabe-Puro plasmid. The following shRNA oligos were used: lacZ shRNA CACCGGGC CAGCTGTATAGACATCTCGAA AGATGTCTATACAGCTGGCCC; TLE3sh1 CACCGCACAAGCAGACAGAGATT GCCGAAGCAATCTCTGTCTGCTTGTGC; and TLE3sh2 CACCGGGCCA GCTGTATAGACATCTCGAAAGATGTCTATA CAGCTGGCCC. Only sense strands are shown.

Luciferase Reporter Assay

10T1/2 cells were seeded in 24-well culture plates at 90% confluence. Cells were cotransfected with 100 ng pGL3-aP2-luciferase or 100 ng PTK-3XPPRE-luciferase and 100 ng pCMX-PPARγ, 20 ng pCMX-RXR, 100 ng pCMX-TLE3, 100 ng pCMX-TLE3(V708D), and 5 ng Renilla control vector using Lipofectamine 2000 (Invitrogen). Forty-eight hours later, cells were treated with DMSO or 100 nM GW7845 in DMEM with 1% FBS for 24 hr. Luciferase activity was determined with STOP&GLO (Promega, Madison, WI) and a GLOMAX luminometer (Promega). Firefly luciferase activity was normalized to Renilla luciferase. Wnt-reporter activity was determined by cotransfecting 50 ng TOPflash reporter, 25 ng constitutively active β-catenin (S37A), 500 ng pCMX-TLE3, and 15 ng Renilla luciferase in 293T cells. Luciferase activity was determined 48 hr after transfection with FuGENE 6 (Roche, Indianapolis, IN).

Gene Expression and Microarray Analysis

Total RNA was isolated using TRIzol reagents (Invitrogen) and reverse transcribed using iScript cDNA synthesis kit (Bio-Rad, Hercules, CA). cDNA was quantified by real-time PCR using SYBR Green (Diagenode, Denville, NJ) and an ABI 7900 instrument. Gene expression levels were determined by using a standard curve. Each gene was normalized to 36B4. Primers used for real-time PCR are listed in Table S5. For microarray experiments, 10T1/2 cells stably expressing CAR ± PPARγ were infected overnight with lacZ or TLE3 expressing adenovirus. Forty-eight hours after infection, cells were stimulated with DMSO or 10 nM GW7845 for 24 hr. RNA was pooled from six biological replicates and processed in the UCLA Microarray Core Facility using GeneChip Mouse Gene 1.0 ST Arrays (Affymetrix, Santa Clara, CA). The results were analyzed using GenespringGX (Agilent, Santa Clara, CA).

Nuclear Extracts

Cells were washed with 1× PBS and incubated with TEN-buffer (10 mM Tris-Cl [pH 8], 100 mM NaCl, 1 mM EDTA [pH 8]). Cells were allowed to swell on ice for 15 min in 10 mM HEPES, 10 mM KCl, 0.1 mM EGTA, 0.1 mM EDTA, 1 mM DTT + complete proteinase inhibitor (Roche). Cells were then mixed with 0.6% NP-40 alternative (Calbiochem, San Diego, CA) for 10 s and centrifuged at 12,000 *g*. Nuclear pellet was resuspended in ice-cold 20 mM HEPES, 420 mM NaCl, 1.5 mM MgCl2, 0.2 mM EDTA, 25% glycerol, 1 mM DTT + complete proteinase inhibitor (Roche). Nuclear extracts were spun at 12,000 *g* for 5 min, and the supernatant was used for further analysis.

Protein Analysis

Proteins were diluted in Nupage loading dye (Invitrogen), heated at 70°C for 20 min, and run on 4%–12% Bis-Tris Gel (Invitrogen). Proteins were transferred to hybond ECL membrane (GE Healthcare, Piscataway, NJ) and blotted using TLE3 (M-201, Santa Cruz Biotechnology, Santa Cruz, CA, or 11372-1-AP, Proteintech Group, Chicago, IL), PPARγ (81B8, Cell Signaling, Danvers, MA), Hmg1 (556528, BD PharMingen, San Diego, CA), TCF4 (C48H11, Cell Signaling), or β-catenin (H-102, Santa Cruz) antibodies. For immunoprecipitation, nuclear extracts were diluted in IP buffer (20 mM Tris, 137 mM NaCl, 2 mM EDTA, 1% NP-40, 10% glycerol) and precleared with Protein A agarose beads (Santa Cruz Biotechnology). Extracts were mixed with IgG (PP64, Millipore, Billerica, MA), TCF4 (C48H11, Cell Signaling), or PPARγ (81B8, Cell Signaling) antibodies and incubated with beads. After spinning, beads were washed with IP buffer and protein-eluted for immunoblotting.

Chromatin Immunoprecipitation

ChIP experiments were performed according to standard protocols (Nielsen et al., 2008). Lysed cells were sonicated using a Bioruptor (Diagenode) according to the manufacturer's protocol, and chromatin was immunoprecipitated with antibodies against TLE3 (11372-1-AP, Proteintech Group), TCF4 (C48H11, Cell Signaling), RNA Pol2 (CTD4H8, Millipore), IgG (PP64, Millipore), β-catenin (610154, BD Transduction Laboratories, San Diego, CA), PPARγ (H-100, sc7196; Santa Cruz Biotechnology or RXR (D197, sc774; Santa Cruz Biotechnology) overnight at 4°C in the presence of Protein A beads (GE Healthcare). DNA enrichment was quantified by real-time PCR (MX-3000, Stratagene, Santa Clara, CA, or ABI 7900, ABI, Carlsbad, CA) using SYBR Green Master Mix (Diagenode or Sigma-Aldrich, St. Louis, MO). Primers used for these studies are listed in Table S4. Occupancy was quantified using a standard curve and normalized to input DNA.

Immunofluorescence

10T1/2 cells were plated in gelatin-treated (0.2%) glass-bottom dishes (Mat TeK Corp., Ashland, MA) and differentiated with DMI + 20 nM GW7845. At day 4 of differentiation, cells were fixed with 4% PFA (1XPBS) and washed with PBS. Cells were permeabilized with 0.1% triton and blocked with 3% BSA. Cells were incubated with TLE3 antibody in 3% BSA overnight, washed, and incubated with Alexa Fluor 555 (A21429, Invitrogen) for 1 hr. After washing, cells were stained with 1 μg/ml BODIPY 493/503 (D3922, Invitrogen) or DAPI (Invitrogen) and washed with PBS. Cells were visualized with LSM 510 confocal laser scanning microscope (Carl Zeiss, Thornwood, NY).

Animal Studies

Male C57BL/6 ob/ob, db/db, and WT littermates were acquired from Jackson Laboratory (Sacramento, CA). Mice were sacrificed at 3 months of age. Transgenic mice were generated at the UCLA transgenic core facility. The −5.4 kb enhancer region of aP2 (Graves et al., 1992) was subcloned into PCR2.1 containing TLE3 cDNA followed by bovine growth hormone polyA (TLE3-PolyA). The linearized construct was gel-purified (Zymol) and microinjected into C57BL/6 fertilized zygotes. Founders were identified by PCR using the following primers: Forward, AGGGAGAACCAAAGTTGAGAAAT, and Reverse, GTCTTCTCGTTTGCCAGCTT. At 12 weeks of age, aP2-TLE3 transgenic mice (F2 generation) and their wild-type littermates were fed a 60% high-fat diet (Research Diets, New Brunswick, NJ) for the indicated times. For glucose tolerance tests, mice were fasted for 6 hr and challenged with an i.p. injection of glucose (2 g/kg). For insulin tolerance tests, mice were fasted for 3 hr and given an i.p. injection of insulin (1 U/kg). Blood glucose levels were monitored using the ACCU-CHEK active glucometer (Roche). Serum adiponectin levels were determined by ELISA (B-Bridge International Inc., Cupertino, CA), and insulin, resistin, and leptin were determined by multiplex immunoassay (Milliplex Kit, Millipore) after 6 hr fast. Body composition and bone mineral density were determined by DEXA analysis. GIR, IS-GDR, and glucose production were determined by euglycemic hyperinsulinemic clamp as described previously (Hevener et al., 2003, 2007; Steele, 1959). No differences in clamp glucose or steady-state insulin concentration were observed between the two genotypes of mice. Indirect calorimetry was performed using a Columbus Instruments Comprehensive Lab Animal Monitoring System (CLAMS, Columbus Instruments, Columbus, OH). Animals were placed individually in chambers for 3 consecutive days at ambient temperature (26.5°C) with 12 hr light/dark cycles. Animals had free access to food and water. Respiratory measurements were made in 20 min intervals after initial 12 hr acclimation period. Energy expenditure was calculated from VO_2 and RER using the Lusk equation, EE in cal/min = (3.815 + 1.232 × RER) × VO_2 in ml/min (McLean and Tobin, 1987). Statistical significance for EE measurements was determined by using two-way ANOVA.

SUPPLEMENTAL INFORMATION

Supplemental Information includes seven figures and five tables and can be found with this article online at doi:10.1016/j.cmet.2011.02.014.

ACKNOWLEDGMENTS

We thank Stephen Young and Karen Reue for helpful discussions and Loren Fong for help with histology. P.T. is an investigator of the Howard Hughes Medical Institute and was also supported by NIH grants HL090553 and DK063491. C.J.V. was supported by NIH training grant HL069766. E.S. was supported by a Career Development Award from the American Diabetes Association, The McDonald's Center for Type 2 Diabetes and Obesity, and NIH grant DK081003.

Received: August 12, 2010
Revised: November 25, 2010
Accepted: January 6, 2011
Published: April 5, 2011

REFERENCES

Arango, N.A., Szotek, P.P., Manganaro, T.F., Oliva, E., Donahoe, P.K., and Teixeira, J. (2005). Conditional deletion of beta-catenin in the mesenchyme of the developing mouse uterus results in a switch to adipogenesis in the myometrium. Dev. Biol. *288*, 276–283.

Bennett, C.N., Ross, S.E., Longo, K.A., Bajnok, L., Hemati, N., Johnson, K.W., Harrison, S.D., and MacDougald, O.A. (2002). Regulation of Wnt signaling during adipogenesis. J. Biol. Chem. *277*, 30998–31004.

Blauwkamp, T.A., Chang, M.V., and Cadigan, K.M. (2008). Novel TCF-binding sites specify transcriptional repression by Wnt signalling. EMBO J. *27*, 1436–1446.

Buscarlet, M., and Stifani, S. (2007). The 'Marx' of Groucho on development and disease. Trends Cell Biol. *17*, 353–361.

Cavallo, R.A., Cox, R.T., Moline, M.M., Roose, J., Polevoy, G.A., Clevers, H., Peifer, M., and Bejsovec, A. (1998). Drosophila Tcf and Groucho interact to repress Wingless signalling activity. Nature *395*, 604–608.

Chen, G., and Courey, A.J. (2000). Groucho/TLE family proteins and transcriptional repression. Gene *249*, 1–16.

Chen, G., Fernandez, J., Mische, S., and Courey, A.J. (1999). A functional interaction between the histone deacetylase Rpd3 and the corepressor groucho in Drosophila development. Genes Dev. *13*, 2218–2230.

Cho, C.Y., Koo, S.H., Wang, Y., Callaway, S., Hedrick, S., Mak, P.A., Orth, A.P., Peters, E.C., Saez, E., Montminy, M., et al. (2006). Identification of the tyrosine phosphatase PTP-MEG2 as an antagonist of hepatic insulin signaling. Cell Metab. *3*, 367–378.

Cho, Y.W., Hong, S., Jin, Q., Wang, L., Lee, J.E., Gavrilova, O., and Ge, K. (2009). Histone methylation regulator PTIP is required for PPARgamma and C/EBPalpha expression and adipogenesis. Cell Metab. *10*, 27–39.

Christy, R.J., Yang, V.W., Ntambi, J.M., Geiman, D.E., Landschulz, W.H., Friedman, A.D., Nakabeppu, Y., Kelly, T.J., and Lane, M.D. (1989). Differentiation-induced gene expression in 3T3-L1 preadipocytes: CCAAT/enhancer binding protein interacts with and activates the promoters of two adipocyte-specific genes. Genes Dev. *3*, 1323–1335.

Combs, T.P., Berg, A.H., Obici, S., Scherer, P.E., and Rossetti, L. (2001). Endogenous glucose production is inhibited by the adipose-derived protein Acrp30. J. Clin. Invest. *108*, 1875–1881.

Dalen, K.T., Schoonjans, K., Ulven, S.M., Weedon-Fekjaer, M.S., Bentzen, T.G., Koutnikova, H., Auwerx, J., and Nebb, H.I. (2004). Adipose tissue expression of the lipid droplet-associating proteins S3-12 and perilipin is controlled by peroxisome proliferator-activated receptor-gamma. Diabetes *53*, 1243–1252.

De Vos, P., Lefebvre, A.M., Miller, S.G., Guerre-Millo, M., Wong, K., Saladin, R., Hamann, L.G., Staels, B., Briggs, M.R., and Auwerx, J. (1996). Thiazolidinediones repress ob gene expression in rodents via activation of peroxisome proliferator-activated receptor gamma. J. Clin. Invest. *98*, 1004–1009.

Debevec, D., Christian, M., Morganstein, D., Seth, A., Herzog, B., Parker, M., and White, R. (2007). Receptor interacting protein 140 regulates expression of uncoupling protein 1 in adipocytes through specific peroxisome proliferator activated receptor isoforms and estrogen-related receptor alpha. Mol. Endocrinol. *21*, 1581–1592.

Freytag, S.O., Paielli, D.L., and Gilbert, J.D. (1994). Ectopic expression of the CCAAT/enhancer-binding protein alpha promotes the adipogenic program in a variety of mouse fibroblastic cells. Genes Dev. *8*, 1654–1663.

Ge, K., Guermah, M., Yuan, C.X., Ito, M., Wallberg, A.E., Spiegelman, B.M., and Roeder, R.G. (2002). Transcription coactivator TRAP220 is required for PPAR gamma 2-stimulated adipogenesis. Nature *417*, 563–567.

Gelman, L., Zhou, G., Fajas, L., Raspé, E., Fruchart, J.C., and Auwerx, J. (1999). p300 interacts with the N- and C-terminal part of PPARgamma2 in a ligand-independent and -dependent manner, respectively. J. Biol. Chem. *274*, 7681–7688.

Graves, R.A., Tontonoz, P., Platt, K.A., Ross, S.R., and Spiegelman, B.M. (1992). Identification of a fat cell enhancer: analysis of requirements for adipose tissue-specific gene expression. J. Cell. Biochem. *49*, 219–224.

Grøntved, L., Madsen, M.S., Boergesen, M., Roeder, R.G., and Mandrup, S. (2010). MED14 tethers mediator to the N-terminal domain of peroxisome proliferator-activated receptor gamma and is required for full transcriptional activity and adipogenesis. Mol. Cell. Biol. *30*, 2155–2169.

Halaas, J.L., Gajiwala, K.S., Maffei, M., Cohen, S.L., Chait, B.T., Rabinowitz, D., Lallone, R.L., Burley, S.K., and Friedman, J.M. (1995). Weight-reducing effects of the plasma protein encoded by the obese gene. Science *269*, 543–546.

Hevener, A.L., He, W., Barak, Y., Le, J., Bandyopadhyay, G., Olson, P., Wilkes, J., Evans, R.M., and Olefsky, J. (2003). Muscle-specific Pparg deletion causes insulin resistance. Nat. Med. *9*, 1491–1497.

Hevener, A.L., Olefsky, J.M., Reichart, D., Nguyen, M.T., Bandyopadyhay, G., Leung, H.Y., Watt, M.J., Benner, C., Febbraio, M.A., Nguyen, A.K., et al. (2007). Macrophage PPAR gamma is required for normal skeletal muscle and hepatic insulin sensitivity and full antidiabetic effects of thiazolidinediones. J. Clin. Invest. *117*, 1658–1669.

Hummasti, S., and Tontonoz, P. (2006). The peroxisome proliferator-activated receptor N-terminal domain controls isotype-selective gene expression and adipogenesis. Mol. Endocrinol. *20*, 1261–1275.

Jennings, B.H., Pickles, L.M., Wainwright, S.M., Roe, S.M., Pearl, L.H., and Ish-Horowicz, D. (2006). Molecular recognition of transcriptional repressor motifs by the WD domain of the Groucho/TLE corepressor. Mol. Cell *22*, 645–655.

Kim, J.Y., van de Wall, E., Laplante, M., Azzara, A., Trujillo, M.E., Hofmann, S.M., Schraw, T., Durand, J.L., Li, H., Li, G., et al. (2007). Obesity-associated improvements in metabolic profile through expansion of adipose tissue. J. Clin. Invest. *117*, 2621–2637.

Kubota, N., Terauchi, Y., Kubota, T., Kumagai, H., Itoh, S., Satoh, H., Yano, W., Ogata, H., Tokuyama, K., Takamoto, I., et al. (2006). Pioglitazone ameliorates insulin resistance and diabetes by both adiponectin-dependent and -independent pathways. J. Biol. Chem. *281*, 8748–8755.

Lehmann, J.M., Moore, L.B., Smith-Oliver, T.A., Wilkison, W.O., Willson, T.M., and Kliewer, S.A. (1995). An antidiabetic thiazolidinedione is a high affinity ligand for peroxisome proliferator-activated receptor gamma (PPAR gamma). J. Biol. Chem. *270*, 12953–12956.

Liu, J., and Farmer, S.R. (2004). Regulating the balance between peroxisome proliferator-activated receptor gamma and beta-catenin signaling during adipogenesis. A glycogen synthase kinase 3beta phosphorylation-defective mutant of beta-catenin inhibits expression of a subset of adipogenic genes. J. Biol. Chem. *279*, 45020–45027.

Louet, J.F., Coste, A., Amazit, L., Tannour-Louet, M., Wu, R.C., Tsai, S.Y., Tsai, M.J., Auwerx, J., and O'Malley, B.W. (2006). Oncogenic steroid receptor coactivator-3 is a key regulator of the white adipogenic program. Proc. Natl. Acad. Sci. USA *103*, 17868–17873.

MacDonald, B.T., Tamai, K., and He, X. (2009). Wnt/beta-catenin signaling: components, mechanisms, and diseases. Dev. Cell *17*, 9–26.

McLean, J.A., and Tobin, G. (1987). Animal and Human Calorimetry (Cambridge: Cambridge University Press).

Moldes, M., Zuo, Y., Morrison, R.F., Silva, D., Park, B.H., Liu, J., and Farmer, S.R. (2003). Peroxisome-proliferator-activated receptor gamma suppresses Wnt/beta-catenin signalling during adipogenesis. Biochem. J. *376*, 607–613.

Molenaar, M., van de Wetering, M., Oosterwegel, M., Peterson-Maduro, J., Godsave, S., Korinek, V., Roose, J., Destrée, O., and Clevers, H. (1996). XTcf-3 transcription factor mediates beta-catenin-induced axis formation in Xenopus embryos. Cell *86*, 391–399.

Nguyen, H., Rendl, M., and Fuchs, E. (2006). Tcf3 governs stem cell features and represses cell fate determination in skin. Cell *127*, 171–183.

Nielsen, R., Pedersen, T.A., Hagenbeek, D., Moulos, P., Siersbaek, R., Megens, E., Denissov, S., Børgesen, M., Francoijs, K.J., Mandrup, S., and Stunnenberg, H.G. (2008). Genome-wide profiling of PPARgamma:RXR and RNA polymerase II occupancy reveals temporal activation of distinct metabolic pathways and changes in RXR dimer composition during adipogenesis. Genes Dev. *22*, 2953–2967.

Park, K.W., Waki, H., Choi, S.P., Park, K.M., and Tontonoz, P. (2010). The small molecule phenamil is a modulator of adipocyte differentiation and PPARγ expression. J. Lipid Res. *51*, 2775–2784.

Puigserver, P., Wu, Z., Park, C.W., Graves, R., Wright, M., and Spiegelman, B.M. (1998). A cold-inducible coactivator of nuclear receptors linked to adaptive thermogenesis. Cell *92*, 829–839.

Qi, C., Surapureddi, S., Zhu, Y.J., Yu, S., Kashireddy, P., Rao, M.S., and Reddy, J.K. (2003). Transcriptional coactivator PRIP, the peroxisome proliferator-activated receptor gamma (PPARgamma)-interacting protein, is required for PPARgamma-mediated adipogenesis. J. Biol. Chem. *278*, 25281–25284.

Roeder, R.G. (2005). Transcriptional regulation and the role of diverse coactivators in animal cells. FEBS Lett. *579*, 909–915.

Ross, S.E., Hemati, N., Longo, K.A., Bennett, C.N., Lucas, P.C., Erickson, R.L., and MacDougald, O.A. (2000). Inhibition of adipogenesis by Wnt signaling. Science *289*, 950–953.

Ross, S.E., Erickson, R.L., Gerin, I., DeRose, P.M., Bajnok, L., Longo, K.A., Misek, D.E., Kuick, R., Hanash, S.M., Atkins, K.B., et al. (2002). Microarray analyses during adipogenesis: understanding the effects of Wnt signaling on adipogenesis and the roles of liver X receptor alpha in adipocyte metabolism. Mol. Cell. Biol. *22*, 5989–5999.

Schoonjans, K., Peinado-Onsurbe, J., Lefebvre, A.M., Heyman, R.A., Briggs, M., Deeb, S., Staels, B., and Auwerx, J. (1996). PPARalpha and PPARgamma activators direct a distinct tissue-specific transcriptional response via a PPRE in the lipoprotein lipase gene. EMBO J. *15*, 5336–5348.

Sekiya, T., and Zaret, K.S. (2007). Repression by Groucho/TLE/Grg proteins: genomic site recruitment generates compacted chromatin in vitro and impairs activator binding in vivo. Mol. Cell *28*, 291–303.

Steele, R. (1959). Influences of glucose loading and of injected insulin on hepatic glucose output. Ann. N Y Acad. Sci. *82*, 420–430.

Steppan, C.M., Bailey, S.T., Bhat, S., Brown, E.J., Banerjee, R.R., Wright, C.M., Patel, H.R., Ahima, R.S., and Lazar, M.A. (2001). The hormone resistin links obesity to diabetes. Nature *409*, 307–312.

Subramaniam, N., Treuter, E., and Okret, S. (1999). Receptor interacting protein RIP140 inhibits both positive and negative gene regulation by glucocorticoids. J. Biol. Chem. *274*, 18121–18127.

Takahashi, N., Kawada, T., Yamamoto, T., Goto, T., Taimatsu, A., Aoki, N., Kawasaki, H., Taira, K., Yokoyama, K.K., Kamei, Y., and Fushiki, T. (2002). Overexpression and ribozyme-mediated targeting of transcriptional coactivators CREB-binding protein and p300 revealed their indispensable roles in adipocyte differentiation through the regulation of peroxisome proliferator-activated receptor gamma. J. Biol. Chem. *277*, 16906–16912.

Tontonoz, P., Graves, R.A., Budavari, A.I., Erdjument-Bromage, H., Lui, M., Hu, E., Tempst, P., and Spiegelman, B.M. (1994a). Adipocyte-specific transcription factor ARF6 is a heterodimeric complex of two nuclear hormone receptors, PPAR gamma and RXR alpha. Nucleic Acids Res. *22*, 5628–5634.

Tontonoz, P., Hu, E., Graves, R.A., Budavari, A.I., and Spiegelman, B.M. (1994b). mPPAR gamma 2: tissue-specific regulator of an adipocyte enhancer. Genes Dev. *8*, 1224–1234.

Tontonoz, P., Hu, E., and Spiegelman, B.M. (1994c). Stimulation of adipogenesis in fibroblasts by PPAR gamma 2, a lipid-activated transcription factor. Cell *79*, 1147–1156.

Tontonoz, P., Hu, E., Devine, J., Beale, E.G., and Spiegelman, B.M. (1995). PPAR gamma 2 regulates adipose expression of the phosphoenolpyruvate carboxykinase gene. Mol. Cell. Biol. *15*, 351–357.

Waki, H., Park, K.W., Mitro, N., Pei, L., Damoiseaux, R., Wilpitz, D.C., Reue, K., Saez, E., and Tontonoz, P. (2007). The small molecule harmine is an antidiabetic cell-type-specific regulator of PPARgamma expression. Cell Metab. *5*, 357–370.

Yamauchi, T., Kamon, J., Waki, H., Terauchi, Y., Kubota, N., Hara, K., Mori, Y., Ide, T., Murakami, K., Tsuboyama-Kasaoka, N., et al. (2001). The fat-derived hormone adiponectin reverses insulin resistance associated with both lipoatrophy and obesity. Nat. Med. *7*, 941–946.

Zelcer, N., Hong, C., Boyadjian, R., and Tontonoz, P. (2009). LXR regulates cholesterol uptake through Idol-dependent ubiquitination of the LDL receptor. Science *325*, 100–104.